1980

The inverse Raman effect: applications and detection techniques

Lester James Hughes Jr.
Iowa State University

HUGHES, LESTER JAMES, JR.

THE INVERSE RAMAN EFFECT: APPLICATIONS AND DETECTION TECHNIQUES

Iowa State University PH.D. 1980

The inverse Raman effect: Applications and detection techniques

by

Lester James Hughes, Jr.

A Dissertation Submitted to the Graduate Faculty in Partial Fulfillment of the Requirements for the Degree of

DOCTOR OF PHILOSOPHY

Department: Chemistry
Major: Physical Chemistry

Approved:

Signature was redacted for privacy.

In Charge of Major Work

Signature was redacted for privacy.

For the Major Department

Signature was redacted for privacy.

For the Graduate College

Iowa State University
Ames, Iowa

1980

TABLE OF CONTENTS

CHAPTER I. THE INVERSE RAMAN EFFECT

Inverse Raman spectroscopy is one of a growing number of non-linear spectroscopic techniques which owe their feasibility to the laser. In general, we may define non-linear in this context as interactions between a photon field(s) and a material medium which occur as a direct consequence of the non-linear terms in the electric susceptibility expansion. The above definition is not a rigid one. Conventional Raman scattering, for example, is not generally considered a non-linear technique since only a single photon is supplied by the external field to the scattering event.

The mechanism involved in inverse Raman scattering is best described by comparing it to the more familiar phenomena of conventional Raman scattering and stimulated Raman scattering. Figure 1 schematically depicts the events occurring in conventional (Fig. 1a), stimulated (Fig. 1b) and inverse (Fig. 1c) Raman scattering.

The initial, $|1\rangle$, and final, $|2\rangle$, states have been chosen to represent vibrational energy states of the molecular system. They are separated by energy E_v.

If the system is irradiated by a photon field, which for convenience is assumed to be monochromatic in Figure 1, it can abstract a photon from the field and pass to an

Figure 1. Molecular processes taking place in (a) Conventional Raman scattering, (b) Stimulated Raman scattering, and (c) Inverse Raman scattering. A wavy line denotes a spontaneous process, a broad line represents a stimulated process.

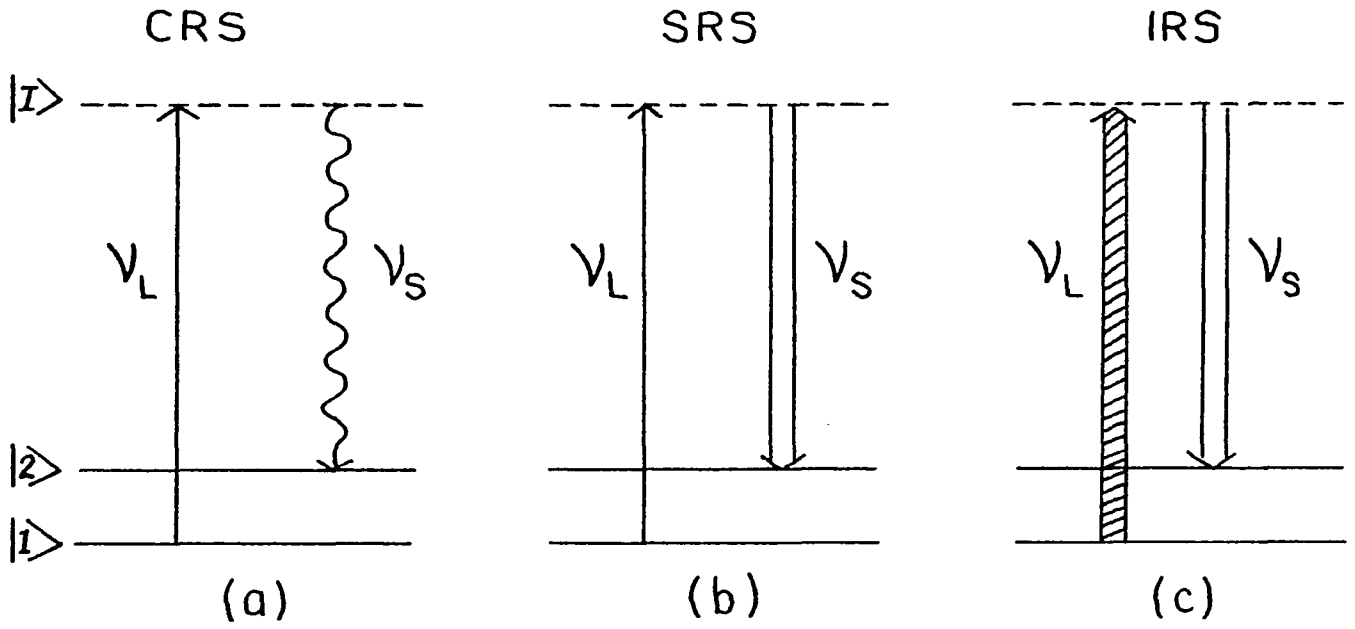
CRS
SRS
IRS
|I>
|2>
|1>
ν_L
ν_S
ν_L
ν_S
ν_L
ν_S
(a)
(b)
(c)

intermediate state $|I\rangle$. The intermediate state may be either a real state (resonance Raman scattering) or a virtual (1) state of the system. We will not treat the resonant case; thus, the intermediate state is dashed to emphasize its virtual nature. Having been excited to the intermediate state, the molecule may undergo one of two general types of scattering: it can scatter (emit) a photon and return to the intial state, or it can scatter a photon which leaves it in a final state which is different from the initial state. In the former case, the scattering is elastic and the energy of the scattered photon is identical to that of the absorbed excitation photon ($h\nu_L$) although the direction of propagation may be different. This elastic scattering, or Rayleigh scattering as it is commonly known, is the dominant scattering process. When the initial and final states are different, the scattered photon will possess energy $h\nu_s$ given by the relationship:

$$h\nu_s = h\nu_L \pm E_v \qquad (1)$$

The minus will obtain in (1) when the final state is an excited state relative to the initial state while the plus will obtain when the converse is true. Historically these two inelastic processes are known as Stokes and anti-Stokes scattering respectively. Since the number of molecules undergoing inelastic scattering will depend upon the

population of the initial state, it is not surprising that the Stokes process dominates the anti-Stokes process.

The description of the scattering processes may have given the impression that the absorption and scattering events are sequential. It must be pointed out that they are temporally inseparable, that is, they occur "simultaneously" and together constitute a single event. (For a discussion of the meaning of "simultaneous" in this context, the reader is referred to page 239 of reference 2.)

From the description of elastic and inelastic scattering, it is obvious that only the inelastic Stokes and anti-Stokes processes provide information about the internal energy structure of the molecule. Less obvious, perhaps, but important in what follows, is the fact that the emission of the inelastically scattered photon in conventional Raman scattering is spontaneous emission. The spontaneous nature of the emission is denoted in Figure 1 by a wavy line while a broad line denotes a stimulated process.

Figure 1b depicts stimulated Raman scattering (3,4) (for convenience only the Stokes case is shown). If the photon field at ν_L is very intense, the photon field generated at ν_s may reach sufficient intensity to induce stimulated Stokes scattering at this frequency. To increase the probability of this occurring, the Raman active medium may be enclosed

in a resonator cavity to enhance the build up of Stokes photons.

Stimulated Raman scattering, unlike conventional and inverse Raman scattering, exhibits a threshold because power losses at ν_s must be overcome in order to reach the stimulated regime. In addition, only strong Raman lines, those with the highest intensity per band width, will go into oscillation while weaker lines will be suppressed. Thus, a stimulated Raman spectrum may appear substantially different from one obtained using the conventional or inverse Raman techniques.

Figure 1c depicts inverse Raman scattering. Only the case analogous to conventional Stokes scattering (i.e., state $|1\rangle$ is the ground state) is treated since this is the situation of interest in the studies to be presented.

The inverse Raman arrangement differs from that of the preceding two techniques in one very important respect, two photon fields, one at ν_L and one at ν_s, are used to irradiate the system instead of the single field at ν_L. The field at ν_L has been a continuum in most applications to date (5-11) although a monochromatic field may be used (12,13) and in some applications is preferable. The field at ν_s is invariably the monochromatic output of a laser.

Certain requirements must be imposed upon the two fields, most important among which are: (1) the fields

must be spatially and temporally coincident in the sample, (2) the field at ν_L (or a frequency component of it, if a continuum) and that at ν_s must satisfy the Raman resonance requirement, i.e., $h(\nu_L - \nu_s) = E_v$, (3) field intensity requirements (to be detailed later) must be satisfied.

In principal the inverse Raman process can readily be grasped. What may be somewhat elusive at this point is the motivation for courting the practical problems that must be inherent in such a technique (to say that all you need to perform inverse Raman spectroscopy are two photon fields of the proper intensities and frequencies coincident in time and space is not unlike the comedian who informed his audience he was going to tell them how to become rich. "First," he said, "go out and get a million dollars"). The justification begins to emerge when one recalls that each Stokes photon created at ν_s in the scattering process is accompanied by the annihilation of an excitation photon at ν_L. In theory the experimenter should have the option of measuring the attenuation of the excitation field at ν_L or the growth of the Stokes field at ν_s. Although many factors affect the intensity of spontaneous Stokes scattering, typical values range from about 10^{-6} to 10^{-8} times the excitation intensity (11,14). It is obvious why the intensity of the Stokes photons is monitored in conventional

Raman spectroscopy rather than attempt to measure the minute attenuation of the strong signal at ν_L. In inverse Raman spectroscopy, on the other hand, by placing the Stokes scattering in the stimulated regime, it is possible to achieve sufficient attenuation of the excitation source to allow absorption at ν_L to be measured. In essence then, inverse Raman spectroscopy is a technique which allows the Raman process to be monitored not in scattering but in absorption. (A more descriptive name for this technique, one which has been used (15) but has not "caught on" is induced absorption at optical frequencies). This leads directly to the question, why is it advantageous to monitor absorption at ν_L rather than scattering at ν_s?

In a conventional Raman arrangement the detector is located at an angle, typically 90^o, to the excitation beam. The collection optics allow one to monitor only a fraction of the scattered photons. Thus a signal that is already weak by virtue of a low quantum mechanical conversion efficiency is rendered even weaker because of the experimental detection scheme. Increasing the interaction path length is of little if any advantage since the experimentally effective path length is defined by the collection optics. When one monitors absorption, however, increasing the interaction path length is an effective method of enhancing a weak response.

If one examines the schematic representations of the various Raman processes in Figure 1 one will observe that the signal of interest in inverse Raman spectroscopy, at ν_L, is on the high energy side of the photon fields while the signal of interest in the conventional technique, at ν_s, is at the low end of the energy spectrum. If either analyte or matrix exhibit fluorescence as a result of the presence of the fields, that fluorescence emission will occur, according to Stokes' law of fluorescence, at lower energies than the excitation energy. One can readily see that fluorescence can, and in practice does, pose severe problems for the conventional Raman spectroscopist whose signal of interest falls within the fluorescence envelope. This problem is obviated by using the inverse Raman technique since one monitors a signal at a frequency which is "upstream" from the fluorescence. Although hot band and resonant fluorescence can interfere at the inverse Raman frequency, the small solid angle required to subtend the entire anti-Stokes beam at ν_L allows a high degree of fluorescence rejection through spatial filtering.

Inverse Raman spectroscopy also holds the potential, as yet unexplored, for increasing the resolution possible in Raman gas phase studies. The Doppler broadening of a Raman line can be expressed as $\Delta\nu_D = C\nu$, where C depends

only upon temperature and molecular weight. The value of ν will vary with the detection geometry and ranges from $(\nu_L + \nu_s)$ for backscattering (180^o), to ν_s for scattering monitored in a conventional geometry (90^o), to $(\nu_L - \nu_s)$ for forward (0^o) scattering monitored in the inverse Raman arrangement. Thus, a reduction in Doppler broadening by the factor $(\nu_L - \nu_s)/\nu_s$ should be afforded by an inverse Raman study relative to a conventional study.

An additional advantage of the inverse Raman technique is that the spectrum can be obtained in the time span of a single laser pulse which, depending on the specific laser, can range from microseconds to picoseconds. Thus, the technique holds great promise as a means for studying short-lived species.

The selection rules for inverse Raman scattering are the same as those of conventional Raman scattering (although it has been suggested (16) that these rules may be relaxed because of the high laser powers used). This fact, coupled with the absence of threshold effects, allows the inverse Raman process to provide spectra identical to that of conventional Raman scattering.

Before surveying the current state of inverse Raman spectroscopy, it will be advantageous to supplement the very qualitative picture which has been presented with a

more detailed, quantitative examination of the underlying principles.

Theory

The information provided by inverse Raman spectroscopy can be divided into two general areas: qualitative (derived from the spectral location of the absorption lines), and quantitative (derived from the degree of absorption). In order to extract quantitative information, therefore, it is necessary to have an expression which allows one to relate the experimentally observed absorption to quantities characteristic of the system under study. This connection, as with most absorption techniques, is via a phenomenological Beer's law type expression which we may write:

$$P_L(\ell) = P_L(0) \exp\left\{-\int_0^{\ell} g(z)\,dz\right\} \qquad (2)$$

where ℓ is the total interaction path length, $P_L(z)$ is the power (watts/cm^2) at ν_L at the indicated depth in the sample and $g(z)$ is the inverse Raman absorption coefficient which, as indicated, is a function of the distance traversed in the sample, z. The dependence of the absorption coefficient on z will be through the power at the Stokes frequency. If the Stokes power is essentially constant throughout the

interaction path length, we can treat the absorption coefficient as a constant in which case equation 2 becomes:

$$P_L(\ell) = P_L(0) \exp\{-g\ell\} \quad (3)$$

Equation 3 allows one to experimentally determine a value for g. If, however, the experimentally determined absorption coefficient is to provide information about the molecular system, we must be able to relate g to experimental and molecular parameters. One may approach the problem of obtaining a theoretical expression for g a number of different ways. The derivation which follows parallels, with some modifications, that of Yeung (11).

The quantum mechanical transition probability per unit time, W_{12}, that a photon with frequency ν_L will be annihilated while simultaneously creating a photon of frequency ν_s and increasing the internal energy of the molecule by $h(\nu_L - \nu_s)$ is proportional to two terms (17):

$$W_{12} \propto \rho(\nu_L)\{\rho(\nu_s) + 8\pi h\nu_s^3 n_s^3/c^3\} \quad (4)$$

where h is Planck's constant (erg-sec), n_s the refractive index of the medium at ν_s, c is the speed of light in vacuum (cm/sec) and $\rho(\nu)$ is the photon energy density per frequency interval at the indicated frequency (erg/cm^3-Hz) (the subscripts L and s will be used throughout consistent with their appearance in Figure 1).

The transition probability per unit time that a photon with frequency ν_s will be annihilated while simultaneously creating a photon of frequency ν_L is proportional to the right hand side of equation 4 with the indices interchanged (s↔L) (5), i.e.:

$$W_{21} \propto \rho(\nu_s)\{\rho(\nu_L) + 8\pi h\nu_L^3 n_L^3/c^3\} \qquad (5)$$

The term $8\pi hn^3\nu^3/c^3$ in the above expressions is responsible for spontaneous emission at the indicated frequency (it can be thought of as the photon energy density due to zero point fluctuations of the vacuum state) while the $\rho(\nu)$ term within the brackets is the photon energy density at the indicated frequency from all other sources. When the dominant photon energy density term in brackets is $8\pi hn^3\nu^3/c^3$, the scattering is spontaneous and one is in the domain of conventional Raman scattering. When the dominant term in brackets is $\rho(\nu)$, the scattering is stimulated and one is in the domain of stimulated and inverse Raman scattering.

Examining equation 4 one can now see why stimulated Raman scattering exhibits a threshold while inverse Raman scattering does not. In stimulated Raman scattering losses in the system must be overcome until the spontaneous Stokes scattering can generate $\rho(\nu_s) > 8\pi hn_s^3\nu_s^3/c^3$. In inverse Raman scattering, on the other hand, the desired inequality

is immediately achieved by externally supplying a large $\rho(\nu_s)$ to the system.

It was stated earlier that the presence of the strong field at ν_s enhances the Stokes scattering (and therefore absorption at ν_L) in the inverse Raman process by placing this scattering in the stimulated regime. One can obtain a quantitative measure of the enhancement by comparing the Stokes scattering rate in inverse Raman scattering to that of conventional Raman scattering.

The Stokes scattering rate, R'_{12}, in conventional Raman scattering is given by:

$$R'_{12} = N_1 W'_{12} \tag{6}$$

where N_1 is the number of molecules in the interaction volume initially in state $|1\rangle$ and W'_{12} is W_{12} (equation 4) in the spontaneous regime. The Stokes scattering rate, R''_{12}, in inverse (stimulated) Raman scattering is:

$$R''_{12} = N_1 W''_{12} - N_2 W''_{21} \tag{7}$$

where N_2 is the number of molecules in the interaction volume initially in state $|2\rangle$ and the double primes indicate the transition rates are evaluated in the stimulated regime.

The enhancement in Stokes scattering at ν_s (and therefore in absorption at ν_L) in inverse Raman scattering relative

to conventional Raman scattering, defined to be γ, is the ratio of the two rates, i.e.:

$$\gamma \equiv R''_{12}/R'_{12} = (N_1 W''_{12} - N_2 W''_{21})/N_1 W'_{12} \tag{8}$$

Equation 8 can be simplified by noting that $W'_{12} \propto \rho(\nu_L) \cdot \{8\pi h n_s^3 \nu_s^3/c^3\}$ and $W''_{12} = W''_{21} \propto \rho(\nu_L)\rho(\nu_s)$. Thus:

$$\gamma = \delta\rho(\nu_s)c^3/8\pi h\nu_s^3 n_s^3 \tag{9}$$

where $\delta = (N_1 - N_2)/N_1$. Using the Boltzmann expression for thermal equilibrium population ratios:

$$\delta = 1 - \exp\{-\Delta\sigma_R/0{\cdot}695T\} \tag{10}$$

where $\Delta\sigma_R(cm^{-1})$ is the Raman shift and T the local (in the interaction region) absolute temperature.

Using the relationship $P_s \cdot 10^7 = \rho(\nu_s)c\Delta\nu/n_s$, where P_s is the Stokes power (watts/cm^2), $\Delta\nu$ the spectral width of the Raman line (FWHM), and converting to vacuum wavenumbers ($\sigma = \nu/c$) equation 9 becomes:

$$\gamma = \delta P_s \cdot 10^7/8\pi hc^2 n_s^2 \sigma_s^3 \Delta\sigma \tag{11}$$

Rigorously one should write $P_s(z)$ in equation 11 since the Stokes power will increase at the expense of $P_L(z)$ as the beam propagates through the medium. However, as will be shown later, under typical experimental conditions, $P_s(0) = P_s(\ell)$ to a high degree of accuracy.

The degree of enhancement in the Stokes scattering rate given by equation 11 can be evaluated for a general case. Using $P_s = 100$ MW/cm^2, $\delta \simeq 1$, $\Delta\sigma \simeq 1$ cm^{-1} and $n_s \simeq 1.5$, one finds $\gamma \simeq 10^6$. The low collection efficiency of conventional Raman spectrometers would render the effective enhancement greater than that given by equation 11. This would be offset to some extent by the superior sensitivity of photon counting over absorption measurements.

Equation 11 gives the degree of enhancement of absorption at ν_L in inverse Raman scattering relative to conventional Raman scattering. In order to obtain an expression for g, it will be necessary to have an expression for this absorption in the conventional process.

An expression which commonly appears in the Raman literature is:

$$P_s = P_L(d\sigma/d\Omega)N\Omega_c\ell \qquad (12)$$

where P_L is the total excitation power (watts), $(d\sigma/d\Omega)$ the differential Raman scattering cross section per molecule per polarization (cm^2/molecule-sr), N the number density of scattering molecules (molecules/cm^3), ℓ the interaction path length (cm), Ω_c the solid angle of collection (sr), and P_s the total Stokes power (watts) scattered into Ω_c. In order to obtain the total Stokes power it is tempting to simply make the substitution $\Omega_c = 4\pi$. However, equation 12 is an

approximation (18) and should be used only when Ω_c is sufficiently small that the differential cross section is essentially constant over Ω_c.

Using the proper differential form of equation 12 and the fact that each Stokes photon created requires the annihilation of an exciting photon, one obtains (19):

$$-dP_L/dz = \{P_L\sigma_L N/\sigma_s\} \int(d\sigma/d\Omega)\,d\Omega \qquad (13)$$

where the integration is over 4π sr.

The absorption in inverse Raman scattering will be greater by the factor γ (equation 11). Thus, we find:

$$-(dP_L/dz)/P_L = g = \{\gamma\sigma_L N/\sigma_s\} \int(d\sigma/d\Omega)\,d\Omega \qquad (14)$$

If the scattering is dipolar, the integral can be evaluated as:

$$\int(d\sigma/d\Omega)\,d\Omega = \frac{8\pi}{3}\,(d\sigma/d\Omega)_o \qquad (15)$$

where $(d\sigma/d\Omega)_o$ is the differential cross section evaluated at 90^o (19). Thus:

$$g(cm^{-1}) = \delta\sigma_L P_s \cdot 10^7 N(d\sigma/d\Omega)_o/(3hc^2 n_s^2 \sigma_s^4 \Delta\sigma)$$

$$= (5{\cdot}6 \cdot 10^{11})(\delta\sigma_L P_s)N(d\sigma/d\Omega)_o/(n_s^2\sigma_s^4\Delta\sigma) \qquad (16)$$

where P_s is expressed in watts/cm^2.

The absorption coefficient may be expressed in terms of frequency $\nu(sec^{-1})$ by multiplying equation 16 by c^4 and by replacing σ with ν, or in terms of cyclic frequency $\omega(rad/sec)$ by multiplying by $(2\pi c)^4$ and replacing σ with ω.

The Stokes power gain in stimulated Raman scattering is phenomenologically described by an expression similar to that for inverse Raman scattering, i.e.,

$$P_s(\ell) = P_s(0) \exp \int_0^{\ell} G(z)dz \simeq P_s(0) \exp \{G\ell\} \tag{17}$$

where $G(cm^{-1})$ is the stimulated Raman gain. Since the increase in the number of Stokes photons per unit interaction path length is equal to the number of photons absorbed from the excitation field per unit interaction length, it is not surprising that the inverse Raman absorption coefficient g is directly related to the stimulated Raman gain G. The relationship may be obtained by any one of several paths. For example, if one takes the differential forms of equations 3 and 17, and uses $P = Nh\sigma c^2/V$ where N is the occupation number of the photon mode and V the beam volume, one obtains:

$$-(dP_L/dz) = -(h\sigma_L c^2/V)(dN_L/dz) = gP_L \tag{18}$$

$$(dP_s/dz) = (h\sigma_s c^2/V)(dN_s/dz) = GP_s \tag{19}$$

Using the fact that $dN_s/dz = -dN_L/dz$, one readily obtains:

$$g(z) = G(z) \{P_s(z)/P_L(z)\}(\sigma_L/\sigma_s) \tag{20}$$

The two ratios which appear in equation 20 may be given the following interpretation. The gain-loss relationship between the fields is directly through the change in field occupation number, not through power (energy) change. Since equation 20 is expressed in power, the factor σ_L/σ_s corrects for the energy discrepancy between photons in the two fields.

The transition probability per unit time for Stokes scattering in the stimulated regime using the field annihilation and creation operator formalism is proportional to two terms (19):

$$W''_{12} \propto N_L N_s \tag{21}$$

where N is the occupation number of the indicated photon mode. Invoking the number balance relationship per unit length one can write:

$$-(dN_L/dz) = (dN_s/dz) \propto N_L N_s \tag{22}$$

If equation 22 is solved for either field as a function of path length, one obtains exponential behavior for both fields with the other field appearing in the exponent, i.e., G will be directly proportional to N_L (and therefore P_L) while g will be directly proportional to N_s (P_s). The ratio

P_s/P_L in equation 20 insures that the correct power term appears in g and G. If only the wavenumber correction is applied to expressions for G (3,4,19-23), g so obtained would be directly proportional to P_L which would assert, quite incorrectly, that the relative attenuation of P_L was a function of P_L.

Expressions for g obtained by other authors directly (11,24,25) and those obtained indirectly from G via equation 20 differ, in general, from that obtained here (equation 16) by factors on the order of unity. The large experimental errors inherent in the measurement of G directly has rendered it difficult to determine which of the theoretical expressions is most accurate. It may indeed be possible to obtain more accurate "gain" measurements indirectly by measuring g which is subject to fewer experimental interferences.

As noted, inverse Raman scattering does not exhibit a threshold. There is, however, a lower limit on the power of the excitation field at ν_L. Figure 1c represents the inverse Raman scattering process where a photon of frequency ν_L is absorbed and a photon of frequency ν_s is scattered. The system will also exhibit a process which is just the reverse of the one depicted, i.e., absorption at ν_s and scattering at ν_L. There will be two sources of this anti-Stokes scattering at ν_L, one spontaneous and one

stimulated. The stimulated contribution has been accounted for by δ in the expression for g. The spontaneous contribution, so far neglected, can serve as a source of interference for absorption measurements at ν_L if P_L is too low. In order to obtain a quantitative measure of this effect it is necessary to reexamine equation 7. If $\rho(\nu_L) \simeq 8\pi h\nu_L^3 n_L^3/c^3$, equation 7 leads to an enhancement γ' given by:

$$\gamma' = \gamma - (N_2/N_1)(n_L\sigma_L/n_s\sigma_s)^3\{\rho(\sigma_s)/\rho(\sigma_L)\} \qquad (23)$$

where γ is the enhancement obtained previously when the spontaneous contribution at ν_L was neglected (equation 9). The negative term in equation 23 represents spontaneous anti-Stokes noise at ν_L and because it is spontaneous the emission will be into 4π steradians. On the other hand, the enhancement represented by γ is due to stimulated emission and will be highly directional. We are interested only in the radiation which emerges in the monitored beam, thus we obtain:

$$\gamma' = \gamma - (N_2/N_1)(n_L\sigma_L/n_s\sigma_s)^3\{\rho(\sigma_s)/\rho(\sigma_L)\}(\Omega/4\pi) \qquad (24)$$

where Ω is the solid angle of collection (generally taken to be equal to the beam divergence) and $\Omega/4\pi$ therefore the fraction of the spontaneous noise that is collected. Equation 24 represents a more general expression for the

scattering enhancement and by substituting γ' for γ in equation 14 one can obtain a more general expression for the inverse Raman absorption coefficient which will be denoted g'. Thus:

$$g' = g(1 - \chi) \tag{25}$$

where g is given by equation 16, $B = \exp\{-\Delta\sigma_R/0{\cdot}695T\}$ $= N_2/N_1$, and χ (dimensionless) is:

$$\chi = 2hc^2 B\Omega\sigma_L^3 n_L^2 \Gamma/\{P_L \cdot 10^7(1 - B)\}$$

$$= (1{\cdot}2 \times 10^{-12})B\Omega\sigma_L^3 n_L^2\Gamma/\{P_L(1 - B)\} \tag{26}$$

Where Γ is the spectral width (cm^{-1}) of either the Raman line ($\Delta\sigma$) or the excitation field (supplying the photons at ν_L) whichever is greater.

If there is to be any absorption at all it is necessary that $1 > \chi$, from which it follows:

$$P_L > (1{\cdot}2 \times 10^{-12})\Omega\sigma_L^3 n_L^2\Gamma\{B/(1 - B)\} \tag{27}$$

Equivalently, one can require that $g > g\chi$, or:

$$P_L > (2/3)(d\sigma/d\Omega)_o(n_L/n_s)^2(\sigma_L/\sigma_s)^4 NB\Omega(P_s/g)(\Gamma/\Delta\sigma) \tag{28}$$

Equation 28 gives numerical values for the minimum P_L in close agreement with those obtained from a similar equation

derived by Strizhevskii and Kondilenko (25) for the case $\Gamma = \Delta\sigma$.

Using equation 27, two different specific cases will be treated. If the Raman active medium is liquid nitrobenzene (σ_L = 15,747 cm^{-1}, $\Delta\sigma$ = 6·6 cm^{-1}, $\Delta\sigma_R$ = 1345 cm^{-1}, T = 300 K, $n_L \simeq 1{\cdot}5$, $\Omega = 10^{-2}$ sr) a P_L of 110 mW/cm^2 is necessary to give g' = 0·99g (i.e., ≃1% error by using g instead of g'). Chloroform vapor ($\Delta\sigma_R$ = 261 cm^{-1}, σ_L = 17,200 cm^{-1}, $n_L \simeq 1{\cdot}5$, $\Delta\sigma \simeq 1$ cm^{-1}, T = 300 K, $\Omega = 10^{-2}$ sr), on the other hand, would require a P_L of 4·1 watts/cm^2 to give g' = 0 99g. Greater power will be required when $\Gamma > \Delta\sigma$.

The Stokes power requirements at the low power limit will be dictated by the minimum absorption that is experimentally detectable. A calculation (11) using typical molecular parameters and a path length of 10 cm indicates that an absorption of 1% will require a P_s of about 25 MW/cm^2 for gas phase samples at atmospheric pressure and about 150 kW/cm^2 for condensed phase samples. Lower concentrations can be compensated by increasing the path length and increasing the Stokes power (e.g., focusing into the sample).

The upper limits on P_L and P_s will be dictated by practical considerations. In general one must avoid powers that are sufficiently high to generate interfering

effects in the medium. Among the interfering processes that can occur are a breakdown of the Raman active medium, localized heating, self-focusing, stimulated Stokes scattering from P_s, stimulated anti-Stokes scattering from P_L, dielectric breakdown and two photon absorption.

Of the possible stimulated scattering effects that can interfere, stimulated Stokes scattering from P_s will, in practice, pose the greater potential problem because of the high Stokes powers generally used. Since stimulated scattering exhibits a threshold, one can void this interference by using a subthreshold P_s. Expressions for the threshold power (19) allow one to estimate the power regime in which such interference can be expected.

Dielectric breakdown (26) is a phenomenon in which suspended particles (generally of micron dimensions) in the medium become photo-conductive in the presence of the intense laser fields. The result of this effect is an anomalous absorption at ν_L. Fortunately this absorption is relatively insensitive to ν_L and, therefore, will be present when ν_L is tuned away from resonance. Careful filtering of the medium will generally suppress the effect.

If the medium possesses a resonance at $2\nu_L$, $2\nu_s$ or $(\nu_L + \nu_s)$, two photon absorption can constitute a significant interference especially if $N(d\sigma/d\Omega)$ is very small (10^{-10} cm^2 sr^{-1} $\gtrsim$) (11). Absorption at $2\nu_L$ can be checked

by measuring the attenuation of P_L in the absence of P_s. Absorption at $2\nu_s$, if present, will generally lead to negligible attenuation of P_s and can be neglected. Absorption at $(\nu_L + \nu_s)$ poses the greatest difficulty to detect experimentally. The presence of fluorescence at frequencies higher than ν_L or ν_s will be indicative of a two photon absorption process. One may also monitor the relative changes in ν_L and ν_s necessary to maintain resonance. The Raman resonance condition can be written, $E_v = h(\nu_L - \nu_s)$, and that for two photon absorption, $E_{tp} = h(\nu_L + \nu_s)$. If resonance is maintained while ν_L and ν_s are changed we obtain, $\Delta\nu_L = \Delta\nu_s$ (Raman) and $\Delta\nu_L = -\Delta\nu_s$ (two photon). Thus, if ν_L is increased (decreased) ν_s will increase (decrease) if the process is Raman scattering; if the process is two photon absorption, as ν_L is increased (decreased) ν_s will decrease (increase).

It is clear from what has been presented that, to a great degree, the utility of the inverse Raman effect as a spectroscopic tool depends upon the availability of an accurate formulation of the inverse Raman absorption coefficient, g. For this reason, the assumptions inherent in equation 16 must be emphasized.

Equation 16 is valid for collimated beams of uniform irradiance in spatial coincidence at all points. Rigorously,

the use of focused laser beams requires radial and axial integration over the fields to correct for the mismatch that can result from their Gaussian nature. However, except when the mismatch in waist diameters in the interaction region is severe, equation 16 provides satisfactory results.

Implicit in the derivation of equation 16 is that the Raman transition is polarized (possesses a depolarization ratio of zero) and that the Stokes laser field is polarized parallel to the excitation field (and therefore parallel to the induced dipole). When dealing with a non-zero depolarization ratio and/or non-parallel polarization of the fields, equation 3 must be amended.

It can be shown (see Appendix C) that equation 3, in the presence of a polarization mismatch in the two fields, and/or a non-zero depolarization ratio becomes:

$$P_L(\ell) = P_L(0)\{e^{-g_1\ell}\cos^2\Theta + e^{-g_2\ell}\sin^2\Theta\} \qquad (29)$$

where Θ is the angle between the polarization vectors of the two fields and ρ is the depolarization ratio. The absorption coefficients g_1 and g_2 represent absorption induced by the components of the Stokes field parallel and orthogonal, respectively, to the excitation field. They are related by the depolarization ratio, i.e.:

$$g_2/g_1 = \rho \tag{30}$$

Straightforward considerations allow these two absorption coefficients to be written:

$$\begin{aligned} g_1 &= g/(1 + \rho) \\ g_2 &= g\rho/(1 + \rho) \end{aligned} \tag{31}$$

where g is given by equation 16. For low absorption, the linearized form of equation 29 is:

$$\Delta P_L/P_L(0) = \{g\ell/(1 + \ell)\}\{\rho + (1 - \rho)\cos^2\theta\} \tag{32}$$

Before closing this section it will be instructive to examine the assumption that the inverse Raman absorption coefficient is essentially constant over the interaction path length, i.e., that $P_s(z) \simeq P_s(0)$. Using equation 20:

$$\int_0^\ell G(z)dz = (\sigma_s/\sigma_L) \int_0^\ell \{P_L(z)/P_s(z)\}g(z)dz \tag{33}$$

Since $G(z) \propto P_L(z)$, and since $P_L(z)$ attenuates as the beam travels through the medium, the maximum value for the Stokes gain occurs just inside the medium where $P_L(z) \simeq P_L(0)$. Thus, the maximum value the integrated Stokes gain may achieve is:

$$\left\{\int_0^\ell G(z)dz\right\}_{max} = G(0)\ell = (\sigma_s/\sigma_L)\{P_L(0)/P_s(0)\}g(0)\ell \tag{34}$$

Equation 34 can be evaluated for a typical situation by using $(\sigma_s/\sigma_L) \simeq 0{\cdot}9$, $P_L(0)/P_s(0) \simeq 10^{-3}$ and $g(0)\ell \simeq 0{\cdot}3$ (a strong absorption). One calculates a maximum integrated Stokes gain of $2{\cdot}7 \times 10^{-4}$. Thus, even though G(z) changes as $P_L(z)$ changes, it is, under the condition that $P_s(0) >> P_L(0)$, sufficiently small at all times that $P_s(z) \simeq P_s(0)$ is an excellent approximation and the use of equation 3 rather than equation 2 is justified. On the other hand, one should recognize the potential error incurred by the use of equation 3 when $P_L(0) \simeq P_s(0)$ (such a situation is treated in Appendix A).

Experimental Methods

As stated earlier, inverse Raman spectroscopy requires two radiation fields spatially and temporally synchronous. The source at ν_s should be spectrally narrower than the Raman line ($<\Delta\sigma$) and of sufficient power to generate measureable attenuation at ν_L. The excitation field may be monochromatic or spectrally broad but must contain frequency components which satisfy the Raman resonance requirement.

The major problem confronting early researchers was obtaining a satisfactory excitation source. The first reported inverse Raman spectrum (5) was obtained using a high power ruby laser and the broad stimulated anti-Stokes emission from toluene. When the ruby field was focused into a cell containing a toluene, a broad "continuum" was generated

centered around $\nu_s + 1003\ cm^{-1}$. Thus, emerging from the toluene cell was the residual ruby field at ν_s and the anti-Stokes continuum containing ν_L. Because of the method of generation, the excitation field was temporally coincident with the ruby. Spatial coincidence was assured by focusing both fields into the sample cell. The absorption was recorded on a photographic plate. This was possible since the temporal width of the excitation field did not exceed that of the Stokes field.

A novel variation of the above method of generating the excitation field was made by Duardo and co-workers (8). They used the same molecule, acetonitrile, as both the source of the anti-Stokes "continuum" and as the abosrbing species. The Raman line at 2940 cm^{-1} was used to generate the anti-Stokes continuum which then served as the excitation field for the line at 2250 cm^{-1}. A similar arrangement has also been used (10) in which two different liquids, one to generate the continuum and one to act as absorber, have been placed in the same cell.

Other sources of the excitation continuum that have been used include the short-lived spontaneous fluorescence of organic dyes resulting from excitation by the second harmonic of the Stokes field (6), and the continuum resulting from self-phase modulation of very intense laser pulses

in liquids and solids (7). The latter technique can provide a continuum which spans the visible spectrum thus, in principle, allowing an entire inverse Raman spectrum to be obtained. However, the continuum is weak and may require multiple laser pulses for proper photographic detection, thus destroying any quantitative information.

An arrangement, first used by Yeung (11), which provides a strong continuum source is shown in Figure 2. A Q-switched ruby laser provides an output of 50-100 MW of radiation at 694 nm (ω_s) in a pulse which is typically 25-30 ns in duration (FWHM). The ruby output passes first through a crystal of potassium dihydrogen phosphate (KDP) which converts a portion of the ruby fundamental to its second harmonic at 347 nm ($2\omega_s$) in a pulse of about 15 ns duration. The ruby fundamental and its second harmonic now enter a network of mirrors, each denoted by M, which have been specially coated to provide selective transmittance/reflectance properties. Mirror 1 serves to separate the spatially coincident ruby fundamental and second harmonic by reflecting the former and transmitting the latter. The second harmonic beam then proceeds to pass through mirrors 2 and 3 and enters a cell containing an organic dye solution. The fluorescence generated in the dye by the absorption of the second harmonic beam builds up and goes into oscillation between mirrors 3 and 6 which form the dye laser cavity. Mirror 6 is totally

Figure 2. Experimental arrangement for inverse Raman spectroscopy using a second harmonic pumped dye laser.

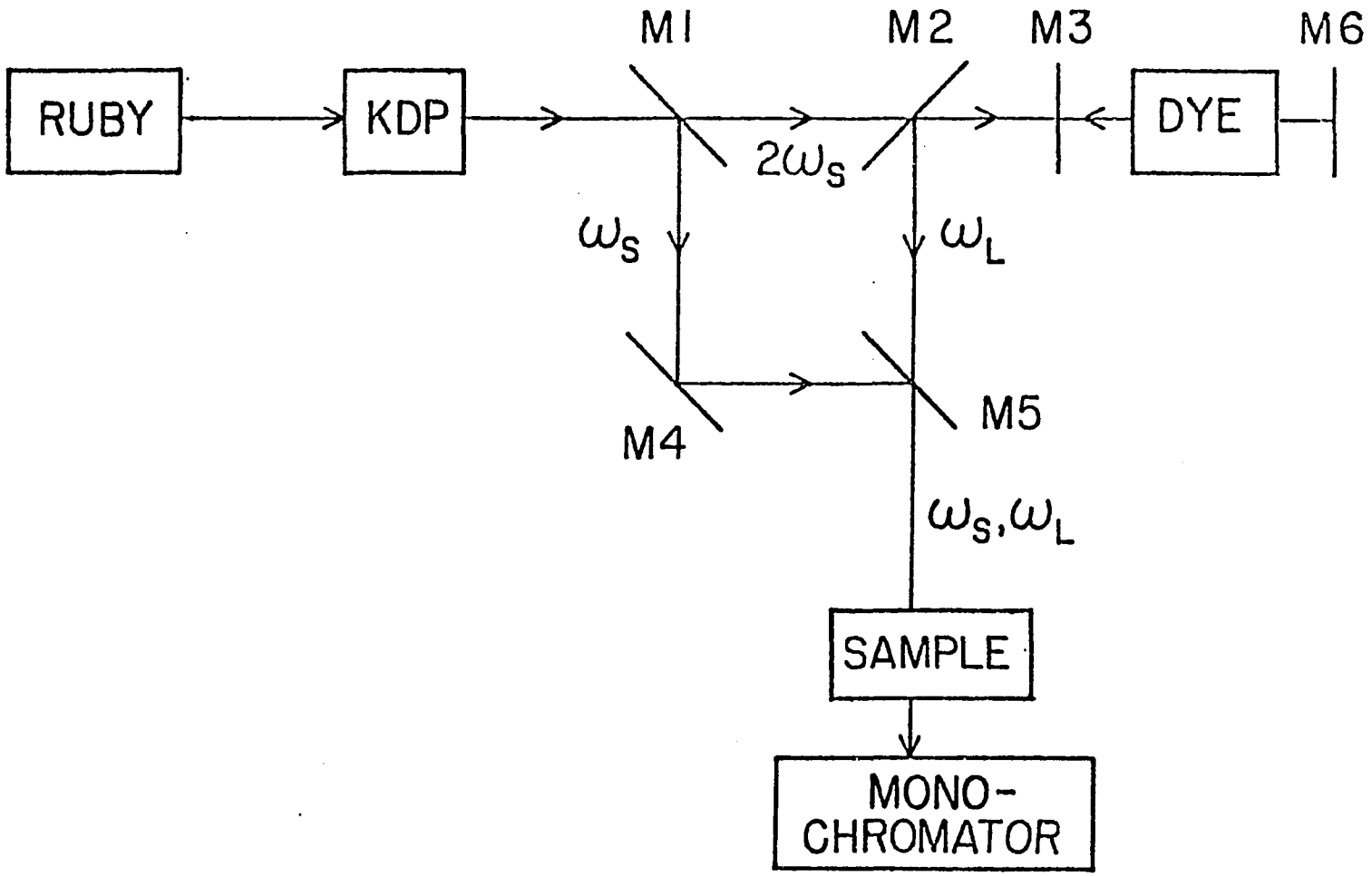
M1
M2
M3
M6
RUBY
KDP
DYE
$2\omega_s$
ω_s
ω_L
M4
M5
ω_s, ω_L
SAMPLE
MONO-
CHROMATOR

reflecting to the fluorescence while mirror 3, which is partially reflecting, serves as the output coupling mirror. The dye laser output (ω_L) is reflected by mirror 2 and transmitted by mirror 5. The ruby fundamental which was separated from the second harmonic at mirror 1 follows what in essence is an optical delay path to mirror 5 via mirror 4. At mirror 5 the intense ruby fundamental (the Stokes field) is united with the broadband output from the dye laser (the excitation field) thus providing spatial and temporal coincidence of the fields and, with proper choice of dye and concentration, satisfying the Raman resonance requirement. The two fields are then typically focused into the sample before passing into a monochromator where the excitation field is separated from the Stokes field and the absorption recorded.

Figure 3 shows the photographic record of the inverse Raman spectrum of the benzene 3065 cm^{-1} line obtained using the experimental configuration of Figure 2 along with a schematic representation of the wavelength and intensity relationships (the intensities are not drawn to scale).

The photograph was obtained by mounting a polaroid oscilloscope camera on a Jarrell-Ash 3·4 meter spectrometer. The magnitude of the absorption can be determined by using a calibrated photographic plate in place of the polaroid camera (11).

Figure 3. Inverse Raman spectrum of the 3065 cm^{-1} line of benzene.

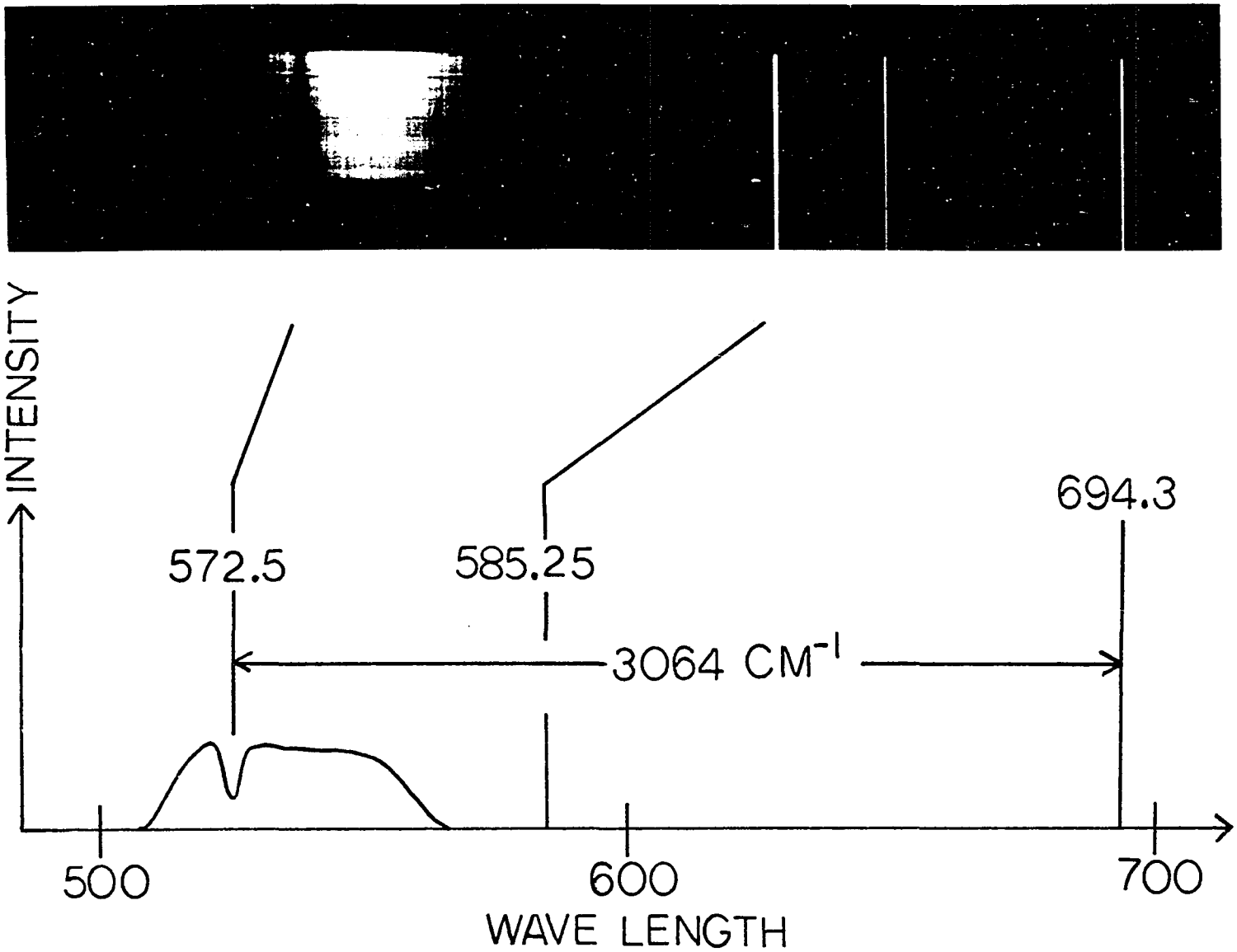
INTENSITY
572.5
585.25
694.3
3064 CM-1
500
600
700
WAVE LENGTH

The photograph shows the broad dye continuum along with sharp lines from a neon discharge lamp which were used for wavelength calibration (the neon line at 585·25 nm is explicitly denoted). Not recorded on the photograph but shown on the schematic is the intense monochromatic Stokes field at 694·3 nm supplied by a giant pulse ruby laser.

The feature of importance in this spectrum is the absorption line which appears in the short wavelength region of the dye continuum. Using the nearest neon line as a wavelength reference and knowing the linear dispersion of the spectrometer, the absorption was shown to occur at 572·5 nm. As shown on the schematic representation, the spectral distance between the Stokes field at 694·3 nm (ν_s) and the absorption at 572·5 nm (ν_L) is equal to the Raman shift of the line, in agreement with theory.

The above schemes rely on photographic detection of the inverse Raman spectrum. This is possible because the temporal width of the generated continuum falls within that of the Stokes pulse. Were this not the case, the absorption line would be washed out by that portion of the continuum at ν_L which was not synchronous with the Stokes pulse.

Although photographic recording is convenient and allows a spectrum to be recorded on the time scale of the laser pulse, the nature of the photographic response can greatly complicate quantitative studies. Improvements in

spectral data acquisition and treatment can be expected with the use of detectors such as vidicons used in a double beam configuration.

Photoelectric time resolved detection will allow the pulsed continuum to be replaced by the output from a cw dye laser. Such an arrangement, and the problems unique to it, will be discussed in Chapter 2.

It would be very convenient to perform inverse Raman spectroscopy using cw lasers for both the Stokes and excitation fields. The feasibility of such an arrangement will depend upon the ability to achieve the power necessary to produce a measurable signal with a cw source. To achieve the power necessary to allow direct absorption measurement would almost certainly require an intra-cavity arrangement using focused beams, an arrangement neither impossible nor straightforward.

The use of cw sources becomes more feasible using detection schemes which, unlike absorption measurements, do not require measuring what may be a small difference between two large signals, but rather allows one to measure a signal against what is essentially a zero background. The two most promising techniques in this area are polarization rotation detection (or RIKES, Raman Induces Kerr Effect Spectroscopy) and photoacoustic detection. These will be discussed later.

Reported Studies

As stated in the first section of this chapter, inverse Raman spectroscopy, because it monitors a signal on the anti-Stokes side of the system, offers high fluorescence rejection compared to a conventional scheme. An excellent example of this capability is provided by the study performed by Werncke et al. (24). Using the inverse Raman technique they were able to obtain spectra of the strongly fluorescing organic dyes rhodamine B and rhodamine 6G. The spectra also exhibited resonant enhancement as one would expect from such strongly fluorescing compounds.

Although, as the above study indicates, high fluorescence rejection is possible in inverse Raman spectroscopy, care must be taken in interpreting the spectra of fluorescing systems since the very presence of fluorescence indicates an abosrption process other than inverse Raman absorption. Conventional one photon absorption from either or both of the fields at ν_L and ν_s, depending on its magnitude, can render interpretation difficult. A sharp one photon absorption from the excitation field can masquerade as an inverse Raman line. Absorption at ν_s will reduce the Stokes power (P_s) in which case quantitative information can be obtained using equation 2 if the exact form of $P_s(z)$ is known (e.g., if the absorption at ν_s is exponential with length and the absorption coefficient is known).

Several studies have been reported in which the ability of inverse Raman spectroscopy to detect the minor component of a mixture was studied. Using a two cell arrangement similar to that of McLaren and Stoicheff (6), Gadow et al. (10) found little if any improvement in detection limits compared to stimulated Raman emission. Attempts to improve detectability by focusing into the sample cell were unsuccessful due to the onset of stimulated scattering. They were, however, able to achieve significantly higher detectability by using a one cell arrangement in which the substance used to generate the anti-Stokes continuum (toluene) was used as the solvent for the minor component. Detectability of the minor component ranged from 5×10^{-3} moles/liter for pyridine to 1.0 mole/liter for aniline and acetophenone.

There have been two main techniques used in an attempt to improve inverse Raman detection limits. The first, resonant enhancement, was mentioned briefly in the discussion of the study of the rhodamine dyes.

The resonance Raman effect (27) is probably the least understood of the scattering processes. Although the perturbation treatments of Raman scattering are not valid in the resonance regime, they do, in a qualitative way, predict what is indeed observed, a large increase in the Raman transition probability as the exciting radiation approaches

resonance with an electronic transition of the molecule. Such an enhancement should compensate for a low concentration for analyte molecules thus improving detectability.

It has been shown (24) in the case of a three level model that in the resonant regime,

$$g \simeq \{(\omega_L - \omega_e)^2 + \Gamma^2\}^{-1} \tag{35}$$

where ω_e and Γ are the resonant frequency and linewidth of the electronic transition. When equation 35 is valid the minimim detectable number density, in the absence of complication from the resonant absorption, is approximately equal to the inverse of g, i.e., $N_{min} \simeq g^{-1}$ (24). If, however, the resonant absorption at ν_s is strong the integrated Stokes power will be proportional to the inverse of the number density thus rendering the absorption coefficient an insensitive function of N. A strong resonant absorption at ν_L may make it impossible to detect the inverse Raman absorption.

Several reports of resonance enhanced inverse Raman studies have been reported (10, 24, 28). Using electronic detection and resonance enhancement it is estimated (24) that the detection of species in concentrations of 10^{-6} moles/liter for typical compounds will be possible.

From equation 16 it can readily be seen that an accurate measurement of the inverse Raman absorption

coefficient will allow the determination of the Raman scattering cross section. Two such studies have been reported, one using a ruby laser and harmonic pumped dye laser and employing photographic detection (11), the other employing photoelectric detection by substituting a cw dye laser for the pulsed dye laser (13).

Little has been done to use inverse Raman spectroscopy to study chemical reactions. The only reported study is that of Von Holle (29) who studied the spontaneous decomposition of a liquid propellant containing isopropyl ammonium nitrate and hydroxyl ammonium nitrate. Using the inverse Raman technique the presence of 2,2-dinitropropane was detected and later confirmed using mass spectroscopy.

Few studies have been reported where the sample was not a liquid. Low gas phase number densities and narrow linewidths require experimental configurations offering both high power and high resolution. Using focusing to achieve a power density of about 1 GW/cm^2, Von Holle (29) was barely able to detect inverse Raman absorption by atmospheric nitrogen.

Although solids offer high number density, they are inherently subject to permanent damage from high power densities. The one solid phase study to date (30) was an extensive study of polaritons in a $LiIO_3$ single crystal.

The well-defined polarization and propagation directions of the fields used in inverse Raman spectroscopy give the technique great potential as a tool in the study of crystalline media.

Inverse Raman spectroscopy is, in theory, capable of higher sensitivity when detection techniques are used which measure the absorption indirectly rather than directly as in the above studies. Using one such technique, photoacoustic detection, a high resolution inverse Raman spectrum of methane was obtained at a pressure of only 50 torr, while detection of the presence of methane extended to a pressure of $1{\cdot}5 \times 10^{-3}$ torr (31). The technique has also been used to obtain the spectra of several neat liquids (32).

CHAPTER II. THE DETERMINATION OF ABSOLUTE RAMAN CROSS SECTIONS

The determination of absolute Raman cross sections has long been as difficult as it was desirous. While the development of the laser represented a giant step forward for the Raman spectroscopist, many problems remained for those who would attempt to measure absolute cross sections.

Accurate absolute Raman cross sections are of great value for a number of areas among which are: providing an understanding of molecular scattering tensors (33); allowing easier quantitative Raman applications such as remote sensing (34); in predicting intensities in coherent anti-Stokes Raman scattering (CARS) (35); in predicting stimulated Raman gain coefficients (36); and in the determination of absolute two-photon absorption cross sections (37).

Photographic recording of Raman spectra of gases and liquids allows the accurate measurement of Raman shifts and, from high-resolution gas phase studies, the accurate determination of molecular constants. However, because of the nature of the photographic response, accurate measurements of Raman cross sections and intensities require the use of photoelectric detection first introduced into Raman spectroscopy by Rank et al. (perhaps in only one study using photographic detection (38) were reliable data obtained). It was not until 1955 that the many necessary

corrections required for careful intensity measurements were considered and applied to the determination of absolute cross sections (39-42).

The development of the laser further reduced the uncertainty in the measurement of absolute cross sections by allowing more accurate determination of excitation intensity and interaction volume. In order to overcome the uncertainties that remained, several techniques have been proposed.

The most reliable gas phase cross sections have been obtained using the J = 1 to J = 3 transition cross section of hydrogen as a reference (43, 44) because its optical anisotropy and wavelength dependence are experimentally and theoretically well-characterized (45-48).

Because of its inertness and ease of mixing with other gases, and because of its use as a standard in air pollution measurements using the Raman LIDAR technique (49), nitrogen is very attractive as a gas phase reference. For this reason, several studies have been undertaken to determine cross sections for the Q-branch of the N_2 vibrational band (44, 50).

Gas phase cross sections have also been obtained by measuring the Raman/Rayleigh intensity ratio (51-53) since accurate theoretical gas phase expressions for the ratio exist.

Because of short range order, intermolecular interactions, and changes in the internal field, the liquid

phase environment is much more complex than that of the gas phase. In general, the cross section for a given Raman line is higher in the liquid state than in the gaseous state (40). In an effort to apply the polarizability theory to liquids, local field correction factors (54, 55) have been incorporated into cross section expressions derived for the gas phase. The complexity of the situation is shown by the fact different lines within the same molecule may undergo different intensity changes upon passing from the gas to the liquid phase even though the internal field correction is the same for all lines within the molecule. This behavior is accommodated within the polarizability formalism by regarding the invariants of the polarizability tensor as functions of intermolecular interactions. It is not surprising, therefore, that unlike the gas phase, there are no theoretical expressions for line intensities in the liquid phase which are sufficiently reliable to allow their use in establishing a reference standard.

In order to establish a liquid phase reference value, a direct absolute cross section measurement was performed on the 992 cm^{-1} line of benzene (56) using a calibrated spectrometer. This value, which suffered from the uncertainties inherent in the calibration process, served as a reference until Kato and Takuma (57, 58) determined absolute

cross sections for several liquids using a black body source as a reference.

There are several major sources of systematic error which confront the spectroscopist in the measurement of Raman intensities: (a) accurate calibration of the response of the detector; (b) determination of the efficiency of the spectrometer; (c) definition of the solid angle of collection; (d) neglect of the angular dependence of the scattering process; and (e) neglect of the temperature dependence of the intensity.

Perhaps the most careful attempt to date to measure an absolute Raman scattering cross section through conventional Raman scattering is the above cited study by Kato and Takuma (57). Using a long focal-length lens they obtained 488 nm output from an argon ion laser in a well-defined excitation beam in the sample. The sample cell utilized oblique plane windows to avoid reflected light contributing to the measured signal. The laser power reflected off the initial cell face was monitored by a calibrated thermopile and used as an index of the power in the cell. The heart of the system was two identical optical systems and rotating sector mirror which alternately projected 1:1 images of the interaction volume and a slit opening of the blackbody source on to the entrance slit of a double monochromator. The laser power was attenuated until a balance, determined by a phase sensitive detector

located at the monochromator exit slit, was achieved between the intensity of the Raman scattering and blackbody radiation. The cross section could then be calculated using a formula derived by these authors.

This experiment arrangement eliminates several sources of error, especially (a), (b), and (c) of those noted previously, but not (d) and (e).

The difficulty in accurately measuring absolute Raman cross sections becomes especially evident when one notes the large discrepancies among reported cross section values from various laboratories. These discrepancies are clear indications of the gap which frequently exists between precision and accuracy.

The potential of inverse Raman spectroscopy for the determination of absolute Raman cross sections was first exploited by Yeung (11). His experimental arrangement is schematically represented in Figure 2. A portion of the output from a giant pulse ruby laser, which provided the Stokes field, was frequency doubled and the resulting field used to pump a dye laser, the output from which provided the excitation field. The two fields were then recombined before passing through the sample and later separated by a monochromator.

Although the use of the inverse Raman technique in that study allowed the elimination of several sources of error,

there were some technical limitations inherent to the arrangement used. The use of photographic detection made quantitation of the absorption difficult. The determination of peak laser powers and the assumptions of perfect temporal coincidence and absence of correlation between spatial modes in the two fields were also sources of uncertainty.

In this chapter an alternative experimental arrangement for inverse Raman spectroscopy which is essentially free of earlier limitations will be described and the results of an experiment using this configuration will be presented.

Experimental

The experimental arrangement used in this study is in many ways similar to those used to measure two-photon absorption (59) or Stokes Raman gain (60). The arrangement is schematically depicted in Figure 4. A ruby laser (R), the output from which provided the intense Stokes field, was passively Q-switched using a solution of vanadyl phthalocyanine in benzene. The ruby laser output was directed first into a 10 cm Raman liquid cell (C) containing nitrobenzene and then into a factory-calibrated Hadron ballistic thermopile (T) by which the shot-to-shot energy was measured. The excitation field was provided by a Spectra-Physics model 581 cw dye laser (D) controlled by a Pockels cell (PC). The

Figure 4. Experimental arrangement used to measure absolute scattering cross section of nitrobenzene. Ruby laser (R); Dye laser (D); Pockels cell (PC); Ballistic thermopile (B); Sample cell (C); Monochromator (S); Photo-tube (P); Oscilloscope (O); Trigger generator (T).

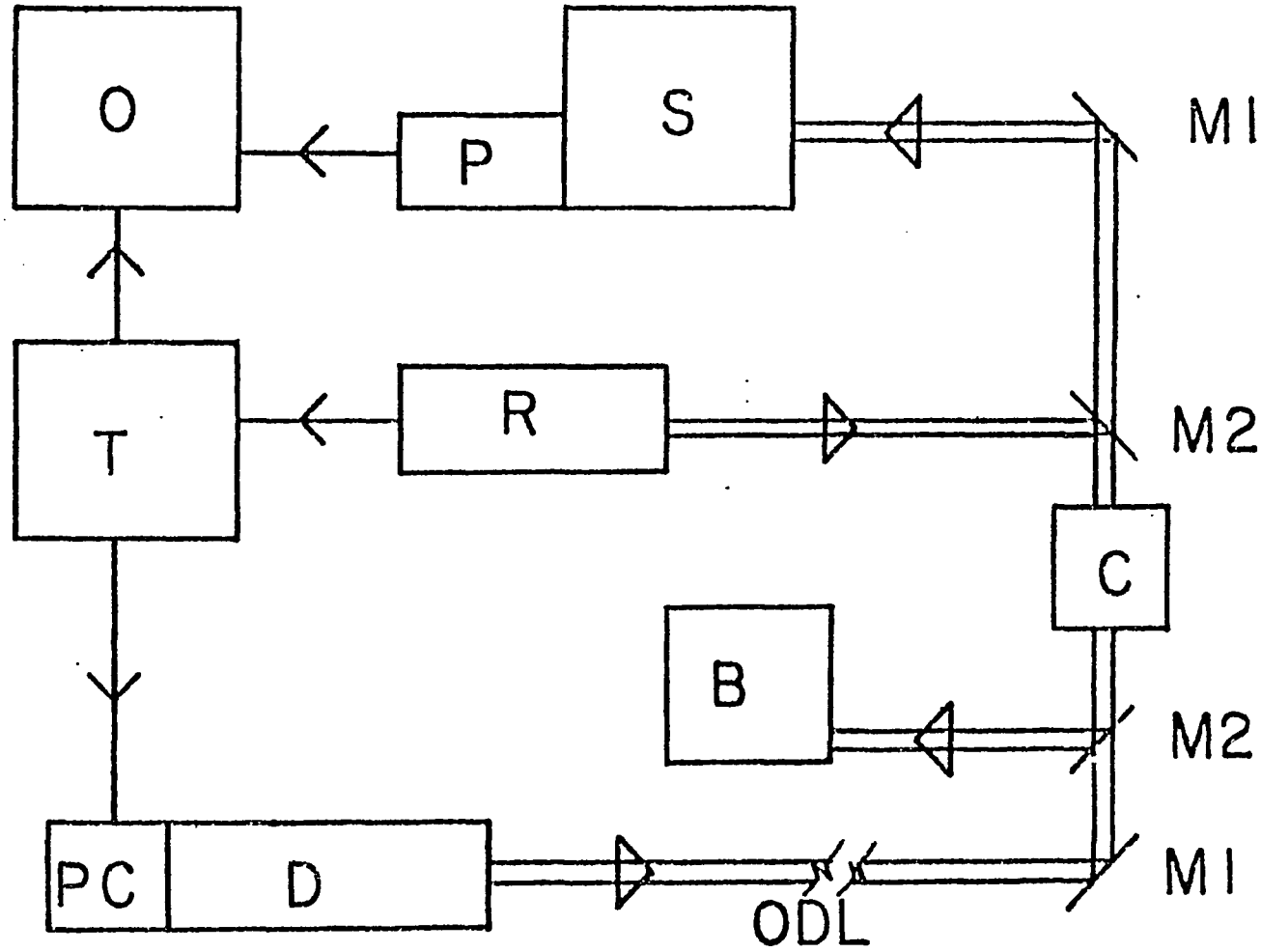
O
P
S
M1
T
R
M2
C
B
M2
PC
D
M1
ODL

dye laser output, expanded ten times with an Oriel B-34-40 beam expander to insure maximum beam overlap, is combined with the ruby field in the Raman cell and then is focused into a Bausch and Lomb double grating monochromator with a spectral slit width of 2·0 nm centered around the dye laser wavelength.

The dye laser intensity passing through the monochromator was monitored with an Amperex 56TVP photomultiplier tube (P) possessing a dynode chain specially designed for high current output, and displayed on a Tektronix 7904 oscilloscope (O) using a 7A19 vertical amplifier. The photomultiplier tube was capable of delivering up to 300 mA while maintaining linearity but only for short light pulses. In order to provide a pulse of appropriate duration from the cw dye laser, a Pockels cell was mounted within the dye cavity. By applying a DC high voltage field to the Pockels cell, using a Lasermetrics GP-4 high voltage pulser, the lasing was quenched by introducing a high loss at the lasing polarization. The firing of the ruby laser activated a trigger generator possessing a variable delay which in turn deactivated the high voltage pulser for a few micro-seconds. During the period in which the voltage to the Pockels was clamped to ground, lasing was achieved thus effectively producing an excitation pulse from the cw dye laser. The

variable delay insured the ability to achieve temporal coincidence.

Results

A problem was encountered early in the study. Mirrors M2, although presenting a very high reflectance to the ruby beam, nevertheless possessed a small but finite transmittance at that wavelength. As a result, a small fraction of the ruby intensity was directed into the dye cavity. The ruby field reaching the dye cavity affected the Pockels cell sufficiently to reduce the gain of the dye laser. To circumvent this effect, an optical delay line (ODL) was introduced by increasing the distance between the dye laser and the Raman cell. By appropriately adjusting the time delay on the trigger generator, the dye laser was fired earlier in order to traverse the increased distance to the cell and arrive at the same time as the ruby pulse. The additional time required for the ruby field to traverse the optical delay line provided a period of unperturbed dye laser output sufficient for any inverse Raman absorption to be detected.

It appeared that inverse Raman absorption was to be achieved in this study with uncharacteristic ease because the very first oscilloscope traces showed a distinct attenuation of the dye field coincident with the arrival of the ruby pulse at the Raman cell (by tuning the monochromator

near the ruby wavelength, the temporal relationship of the ruby pulse to the dye output could be determined from the ruby intensity scattered from the cell window). Unfortunately, the absorption persisted when the dye laser was tuned away from the Raman resonance. The observed behavior was consistent with the phenomenon of dielectric breakdown (26). This off-resonance absorption disappeared after careful filtering of the nitrobenzene.

An inverse Raman absorption was then recorded and confirmed by the fact that the absorption was coincident with the ruby pulse, and that the absorption disappeared when the dye laser was tuned off resonance or when the ruby field was blocked before entering the cell.

A typical oscilloscope trace of the inverse Raman absorption is shown in Figure 5. The vertical axis represents dye laser intensity and increases from top to bottom. The horizontal axis represents time (50 ns/division) and increases from left to right. The dot at the upper left margin represents zero intensity output from the photomultiplier tube. The Pockels cell was switched off and the dye laser switched on several microseconds before the trace to allow stabilization of the dye laser output to the value recorded at the beginning of the trace. The first drop in the dye laser intensity, the peak of which occurs about 70 ns into the trace, represents the inverse Raman absorption

Figure 5. Oscilloscope trace of inverse Raman absorption. Time axis, 50 ns/division.

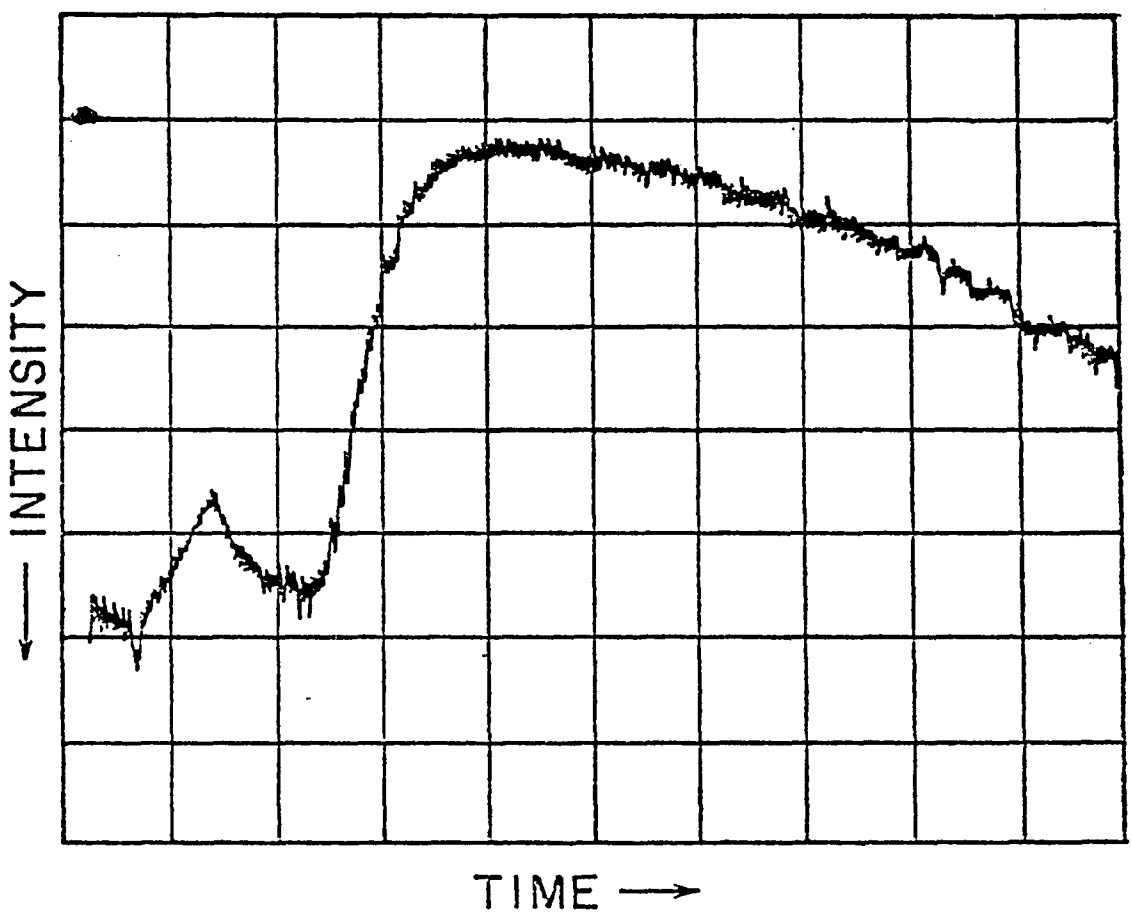
INTENSITY
TIME

and is coincident with the ruby pulse. About 50 ns after the peak of the inverse Raman absorption, the dve laser intensity begins to drop again. This attenuation is coincident with the arrival of the ruby pulse in the dye cavity. Had an optical delay line not been used, this second strong and rather long-lived drop in intensity would have occurred earlier and obscured the inverse Raman absorption.

In order to determine the absolute Raman cross section, the inverse Raman absorption coefficient, g, must first be obtained via equation 3. Once a value for g is determined, the absolute Raman cross section can be extracted from equation 16. Combining these equations we obtain:

$$(d\sigma/d\Omega)_0 = (K/\ell P_s)\log_e\{P_L(0)/P_L(\ell)\} \tag{36}$$

where K contains terms characteristic of the system under study and is given by:

$$K(\text{watts-cm-sr}^{-1}) = (1.79 \times 10^{-12})(n_s^2\sigma_s^4\Delta\sigma)/(\delta\sigma_L N) \tag{37}$$

For low absorption, equation 36 can be written:

$$(d\sigma/d\Omega)_0 = (K/\ell P_s)\{\Delta P_L/P_L(0)\} \tag{38}$$

The number density, N, is calculated from density data to be 5.86×10^{21} cm^{-3}. The index of refraction, n_s, is

taken to be 1·54 (61). The values of σ_s and σ_L are 14402 cm^{-1} and 15747 cm^{-1}, respectively. A Raman linewidth, $\Delta\sigma$, of 6·6 cm^{-1} (measured by conventional Raman spectroscopy) was used (19). The value of δ at room temperature is essentially unity.

In principal, any value of $P_L(0)$ and $P_L(\ell)$ at any given time on the absorption curve could be used to obtain g if the proper value of P_s at that time were known; it is most convenient to measure the peak absorption. Thus $P_L(0)$ and $P_L(\ell)$ are obtained directly from the oscilloscope trace. The Stokes power associated with the peak absorption is obtained by dividing the energy of the ruby pulse measured by the ballistic thermopile (corrected for reflection losses at surfaces) by the temporal width of the pulse at half maximum absorption. The duration of the ruby laser pulse is not reproducible from one trial to the next and, like the Stokes energy, must be measured for each trial. The pulse width varied by as much as 20% in this study.

Using equation 36 and correcting for a non-zero depolarization ratio of 0·15 (56), the data from 65 spectra yield an absolute Raman scattering cross section of (2·35 ± 0·27) $\times 10^{-29}$ $cm^2 sr^{-1}$ for the 1345 cm^{-1} line of nitrobenzene. The indicated uncertainty includes realistic estimates of the accuracies of the individual parameters, particularly the calibration of the thermopile, the contribution of the

finite width of the oscilloscope trace to errors in measuring intensity, and the accuracy of the pulse width measurements from the individual photographs. Measurements of the last two parameters, relative intensity and pulse width, represent the most significant sources of error in this study.

When the spectral bandpass of a conventional Raman spectrometer is sufficient to allow detection of radiation scattered from the entire line, the cross section measured is the integrated scattering cross section $(d\sigma/d\Omega)_i$. By closing the spectrometer slits and operating at high resolution, the intensity at line center and its associated cross section, the peak cross section $(d\sigma/d\Omega)_p$ can be determined. The two cross sections are related, for a Lorentzian profile, by

$$(d\sigma/d\Omega)_i = (\pi\Delta\sigma/2)(d\sigma/d\Omega)_p \qquad (39)$$

Equation 39 yields a peak cross section per molecule for the 1345 cm^{-1} nitrobenzene line of $2{\cdot}77 \times 10^{-30}$ cm^3 sr^{-1}.

Discussion

It was claimed in the introduction to this chapter that using inverse Raman spectroscopy to measure absolute Raman scattering cross sections offered advantages over conventional techniques. To show that this method is indeed more reliable, the various possible sources of inaccuracies will be considered in detail.

The angular dependence of the Raman scattering process has been properly taken care of in the inverse Raman technique. The lasers have a beam divergence of less than 5 mrad and are aligned to be propagating at $180^{o} \pm 1^{o}$. This is far better than the solid angle subtended by the collection optics of a typical Raman spectrometer where it is assumed that all collected light represents 90^{o} scattering.

The short pulse durations of the two fields and the larger cross-sectional areas of the beams used in this study should reduce the extent of sample heating relative to typical laser Raman studies and thus minimize temperature effects on the intensity.

Both lasers provided fields of sufficient spectral resolution (the dye laser field, the spectrally broader of the two fields, possessed a width of less than 1 cm^{-1}) relative to the 6·6 cm^{-1} width of the Raman line that the shift between the two fields could be centered at the peak of the transition by maximizing the normalized absorption. Thus, any error due to inaccuracies in the absolute frequencies of the fields (e.g., a temperature shift of the ruby) would not be sources of error.

Complete spatial overlap of the two lasers was assured in this arrangement. The diameter of the ruby beam was 0·9 cm and that of the expanded dye beam 0·5 cm. The dye field was therefore completely covered by the ruby field

even if slight misalignment is present. Furthermore, the single mode (TEM_{00}) property of the dye laser field smooths out the multimode nature of the ruby field so that only the average power across the whole beam needs to be determined. Mathematically, this is equivalent to taking a slowly varying function (the dye laser power spatial dependence) outside of the integral over the product of the field powers thus leaving only the ruby field power to be spatially integrated. This offers a more satisfactory approach to dealing with the multimode properties of lasers than earlier work (11).

Because one source is a cw laser, temporal coincidence of the two lasers is assured. Problems in synchronizing the two fields are entirely eliminated. It may be noted that a detailed study of the time dependence of the two fields has been neglected in this study. The ruby laser may in fact be partially mode-locked and the dye laser field probably contains high frequency components resulting from the beating of longitudinal modes. Although ideally one would like to use a single longitudinal mode cw dye laser, mathematical modeling shows that as long as the temporal behavior of the two fields is uncorrelated, the photo detector will average out such fluctuations.

The determination of the power density P_s for each trial in this arrangement is reliable since spatial and

temporal fluctuations will be averaged out as discussed above. A question that does remain is, what is the effect of slow detector response on experimental accuracy? That is, how can the peak power be measured to correlate with the peak absorption if the detector is slow compared to the temporal features of the laser pulse? Since $P_L(0)$, $P_L(\ell)$, and the laser pulse width, and therefore the peak P_s, are determined from the same oscilloscope trace, a slow photo detector will respond to indicate a smaller absorption whenever it underestimates the peak laser power (assuming the pulse area is proportional to pulse energy). To estimate the error introduced by such a situation, we assume that equation 3 can accurately be approximated by a truncated expansion (the observed integrated absorption coefficients in this study could be approximated to better than 0·5% by an expansion through second order). We thus obtain:

$$\{\Delta P_L/P_s\}/P_L(0) = g'\ell - (g'\ell)^2 P_s/2 \qquad (40)$$

where $g = g'P_s$. The left hand side of equation 40 is independent of error since a slow detector underestimates both ΔP_L and P_s to the same extent and the effects cancel. Error will be introduced in equation 40, therefore, only from the term containing P_s on the right hand side. If the absorption

is sufficiently small so that this term is negligible in the expansion, the experimental results will be insensitive to slow detector error. Even if the term containing P_s in equation 40 must be included, the error will be relatively small for moderate slow detector error. For example, if the slow detector leads to a low Stokes power P_s' which is related to the actual Stokes power, P_s, by $P_s' = P_s(1 - \varepsilon)$, an error term of $\varepsilon(g'\ell)^2 P_s/2$ will be introduced in the right hand side of equation 40. Using typical values encountered in this study we find:

$$\{\varepsilon(g'\ell)^2 P_s/2\}/\{\Delta P_L/P_s P_L(0)\} \simeq 0{\cdot}15\varepsilon \qquad (41)$$

Using equations 40 and 41 to calculate g', one finds an error of about 3·5% for $\varepsilon = 0{\cdot}2$ and 9% for $\varepsilon = 0{\cdot}5$ (the calculated value of g', and hence the cross section, will be too low). Thus, this experimental approach reduces the sensitivity of the calculated absorption coefficient to slow detector error.

Several modifications are possible which would further reduce experimental uncertainties. By introducing a dc bias to the signal and expanding the scale more accurate absorption measurements should be possible. In addition, the use of a second oscilloscope used solely to monitor the laser pulse should provide more reliable pulse duration values.

CHAPTER III. ALTERNATE METHODS OF DETECTION

The sensitivity of inverse Raman spectroscopy is determined to a large degree by the technique used to measure the absorption. Direct absorption measurement, the most obvious and perhaps the most straightforward technique, in principal offers less sensitivity than other available methods. These other methods, while affording greater potential sensitivity, are not without their own special problems and limitations. This chapter will detail the efforts to employ three of these techniques.

Photo-acoustic Detection

Although the photo-acoustic effect has been known for a century (62), it was not until the development of the laser that its full potential as a spectroscopic tool could be utilized.

In principal the photo-acoustic effect can readily be understood. If electromagnetic radiation is passed through a gas which possesses a finite absorption coefficient for the radiation, a fraction of the radiant energy will be absorbed. Assuming for simplicity that the molecules possess only two energy levels, those which are in an excited state can return to their ground state via three paths: re-radiation of a photon; collisional resonant energy transfer to a molecule of the same species initially in its ground

state in which case the total internal energy of the colliding molecules is conserved; a collisional energy transfer in which the internal energy of the excited molecule is degraded into translational energy for the colliding molecules. The third process results in increased heat energy and therefore an increase in the local pressure. If the radiation is modulated at a rate slower than the collisional relaxation process, the temperature and hence the pressure increase will also be modulated at the same rate. If the modulation is at audio frequencies (generally from about 20 Hz to 20 kHz) a microphone can be used to detect the pressure (sound) wave.

One can see from the above that the photo-acoustic spectrum of a substance will reflect the absorption spectrum of that substance, although in real molecules the situation is obviously more complex because of the various relaxation processes that may be available to the molecule.

The high sensitivity of photo-acoustic detection derives from the fact that, as with fluorescence, one is monitoring a signal against what is ideally a zero background, and because the modulated excitation allows extraction of the signal with phase sensitive detection. Using photo-acoustic detection absorption coefficients of 10^{-7} cm^{-1} have been reported (63).

Although the bulk of photo-acoustic studies have been performed on gas phase samples, considerable attention has recently been devoted to solid (64) and liquid samples (65). When using condensed samples a coupling gas is generally used as a conduction medium to allow the generation of a pressure wave.

The application of photo-acoustic detection to non-linear Raman absorption has been reported in the gas phase using both cw (31) and pulsed laser excitation sources (66), and in the liquid phase using a pulsed source (32). One can show (see Appendix B) that the pressure change induced by inverse Raman absorption is given by:

$$\Delta p(J/cm^3) = (\gamma - 1)A\tau P_L(0)g\ell\Delta\sigma_R/\sigma_L V \qquad (42)$$

where $A(cm^2)$ is the cross sectional area of the interaction region, $\ell(cm)$ the interaction length, $\tau(sec)$ the interaction time, γ is the heat capacity ratio (C_P/C_V) of the gas in which the pressure wave is generated, $\Delta\sigma_R(cm^{-1})$ is the Raman shift of the state populated by the inverse Raman absorption, $\sigma_L(cm^{-1})$ is the energy of an excitation photon, $V(cm^3)$ is the cell volume, $P_L(0)$ is expressed in watts/cm^2, and $g(cm^{-1})$ is given by equation 16.

From the above equation it is obvious that an accurate measurement of the pressure change resulting from inverse

Raman absorption will allow one to readily obtain the same information available through absorption measurements but with the higher sensitivity of photo-acoustic detection.

The initial attempt to photo-acoustically detect inverse Raman absorption was made under substantially less than ideal conditions. Our laboratory possessed both a cw argon ion (Ar^+) laser and a tunable cw dye laser which together would have been excellent radiation sources for the proposed experiment (in fact the first reported photo-acoustic detection of inverse Ramna absorption (31) utilized such an arrangement). Unfortunately, the dye laser required the Ar^+ laser as an excitation source. Thus, the use of one precluded the use of the other.

Confronted with this limitation, it was decided to use the Ar^+ laser alone. Using a Littrow prism, the Ar^+ laser can be tuned to emit any one of six possible wavelengths ranging from about 458 nm to 515 nm. If the prism is replaced with a broadband mirror, all six lines will be emitted simultaneously. A search was therefore conducted for substances which met three criteria: a Raman shift equal to the difference between any two of the stronger Ar^+ laser lines; high Raman cross section; high vapor pressure. Since the experiment would be conducted on gas phase species, the last criterion would assure a reasonable number density of

scattering molecules. As a result of the above considerations, thiophene and methyl acetate were chosen for the study. Both exhibit a Raman resonance at about 845 cm^{-1}, the difference between the 496·6 nm and 476·6 nm Ar^{+} laser lines.

The cell was constructed of polished Plexiglas to maximize the transmission of scattered light out of the cell and away from the microphone where its absorption by the diaphragm would constitute an interference. To further reduce the access of scattered light to the microphone, the microphone was offset below the bore of the cell. The cell windows were a matched pair of plano-convex lenses designed to bring the radiation to a focus in the center of the cell and re-collimate it as it left the cell. The distance between the lenses was about 5.5 cm and the diameter of the cell in the focal region about 9 mm.

To detect the generated pressure wave, a 1/4" B & K microphone and pre-amp were sealed using an o-ring arrangement into the Plexiglas block housing the cell. The output from the pre-amp was fed to a B & K variable gain amplifier and then into an Ortec lock-in amplifier. A Princeton Applied Research variable speed chopper was used to modulate the laser radiation.

Using a helium leak tested valve attached to the cell, the cell was evacuated to a pressure of about 10^{-3} torr and

the sample vapor then allowed to equilibrate in the cell which was then sealed.

Both samples produced a definite photo-acoustic signal which decreased, as expected, with increasing chopping rate. However, the experimental arrangement, that of providing both excitation and Stokes fields from the same Ar^+ laser, ruled out the two primary ways of confirming the presence of an inverse Raman process, i.e., blocking one field or tuning away from the Raman resonance. In an effort to see if the signal was the result of other processes the experiment was repeated using a single Ar^+ line on the samples, and the broadband Ar^+ laser output with the cell evacuated, and containing air.

Based on the results of these tests, it was concluded that either the inverse Raman signal was being lost in window and scattered light noise, or that inverse Raman absorption was not taking place. Calculations based on equation 42 using estimated cross section values indicate that a very stable, low noise arrangement would allow detection of the signal if exact resonance were achieved. Because of the paucity of gas phase Raman data available, liquid phase spectra (67) were used as a guide. The shifting and narrowing of gas phase lines relative to the liquid phase made resonance uncertain. The unavailability of a

conventional laser Raman spectrometer made it impossible to determine the location of the lines in the gas phase.

Considering the limitations imposed by the available equipment, the lack of success in this experiment was not surprising. Barrett and Berry (31) used an intra-cavity arrangement utilizing an Ar^+ laser and tunable cw dye laser in the first successful experiment to photo-acoustically detect inverse Raman absorption. The higher power and increased latitude in sample choice afforded by their arrangement provided a signal, based on equation 42, which was two hundred times greater than that which we would have ideally seen.

In an effort to reap the benefits of a tunable source, a Chromatix CMX-4 tunable pulsed dye laser was borrowed and used with the cw Ar^+ laser to study benzene. The same cell used in the previous study was again used. The experimental arrangement is shown schematically in Figure 6.

The dye laser (D) providing the Stokes field (σ_S) and the Ar^+ laser (A) providing the excitation field (σ_L) were counter-propagated into the photo-acoustic cell (PC). The generated pressure wave was detected by the microphone (M) and the signal fed successively to an audio amplifier (AA) and a phase sensitive detector (L). A "synch-out" gate available on the dye laser provided a reference signal for

Figure 6. Experimental arrangement for photo-acoustic detection. Pulsed dye laser (D); Ar^+ laser (A); Photo-acoustic cell (PC); Microphone (M); Audio amplifier (AA); Lock-in amplifier (L).

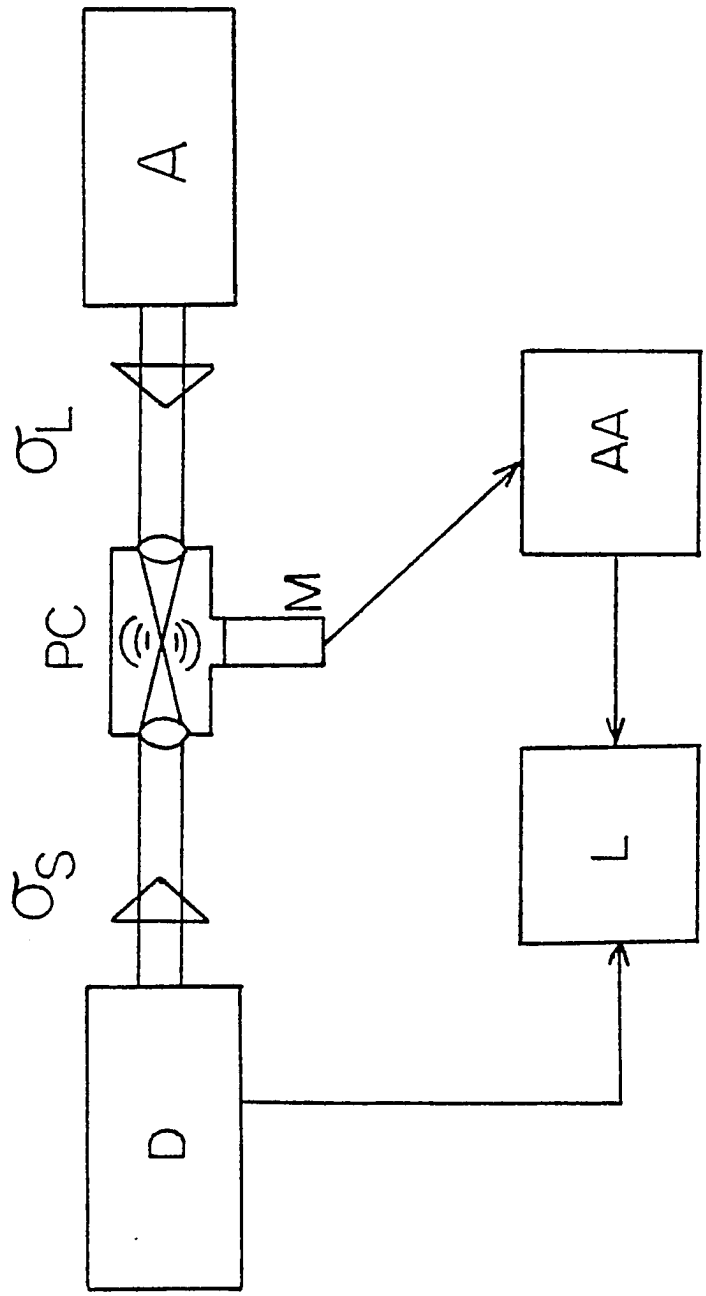
A
σ_L
PC
M
AA
L
σ_S
D

the lock-in amplifier (L) thus obviating the need for a mechanical chopper.

The dye laser was tuned to the benzene Raman shift of 3069 cm^{-1} (68) relative to the 514·5 nm line of the Ar^+ laser. The Ar^+ laser provided power of about 2·5 watts cw while the dye laser, using Rhodamine 6G, provided peak powers of about 3 mJ in pulses of 1 μsec duration at rates up to 30 pulses/sec. The dye laser power at the focal point was estimated to be approximately 300 kw/cm^2.

Slow scanning (0·01 cm^{-1}/sec) through the resonance region failed to produce an unambiguous, stable photoacoustic signal. An analysis of the arrangement reveals that the problem resides with the dye laser source which, although it provides tunability and increased peak power, possesses too low a duty cycle to allow adequate excitation. This can be seen by examining equation 42. The pulse width of the laser gives τ a value of 10^{-6} sec., equivalent, from the standpoint of energy deposited in the sample, to a mechanical chopping rate of 1 MHz. Equation 42 and the microphone sensitivity (≈10 mV/PA) lead to an estimated unamplified signal of 0·2 μV which, using an amplifier and phase sensitive detection, should be detectable but only if the system were stable and essentially free of resonant noise. Considering the magnitude of the expected signal and our inability to

extract a signal which met the criteria for inverse Raman absorption, it is believed that resonant signals from absorption by the windows probably masked any signal of interest.

One fact which was made painfully obvious by the above experiments was that high laser power would greatly enhance the chance of success in such a study. For this reason, attention was focused on the higher power pulsed lasers available in our laboratory, specifically, a giant pulse ruby laser and a Phase-R model D-2100 flash lamp pumped dye laser.

The ruby laser can provide power up to about 100 MW/cm^2 without focusing in pulses of 25 to 35 nsec. In order to provide high power in both the excitation and Stokes fields during the pulse and to assure temporal coincidence of the two fields an experiment was designed that would allow the ruby laser output to directly provide the excitation field and indirectly, by generating stimulated Raman scattering, to provide the Stokes field.

The experimental arrangement used is shown schematically in Figure 7. The output (σ_L) from a passively Q-switched ruby laser (R) was directed into a cell (GC) containing a hydrogen/helium mixture at a total of 600 psi. The cell was specially designed to withstand such pressures and to allow adjustment of the inter-window distance. The windows

Figure 7. Experimental arrangement for photo-acoustic detection. Ruby laser (R); Stokes generating cell (GC); Photo-acoustic cell (PC); Microphone (M); Ballistic thermopile (T); Amplifier (A); Oscilloscope (O).

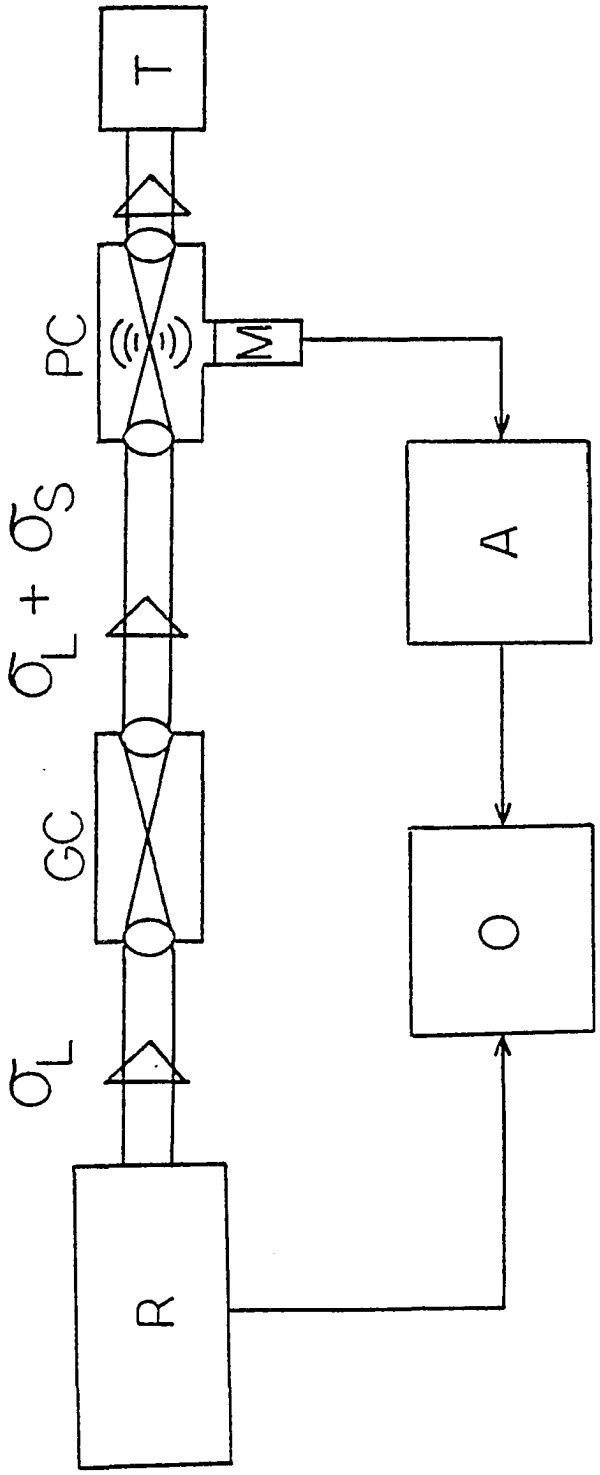
T
PC
M
A
$\sigma_L + \sigma_S$
GC
O
σ_L
R

were matched plano-convex lenses designed to bring the laser radiation to a focus in the cell and then recollimate it as it leaves the cell. With the cell filled, optimum recollimation was achieved by passing the radiation from a He/Ne laser through the cell and changing the inter-window distance while watching the far field size of the He/Ne beam.

The intense ruby field at the focal point, enhanced by the high number density of a partial pressure of about 500 psi, leads to the generation of intense stimulated Raman scattering by the hydrogen (conversion efficiency $\simeq$ 25% (69)) providing a Stokes field (σ_S) with a photon energy (cm^{-1}) of ($\sigma_L - \Delta\sigma_H$) where $\Delta\sigma_H$ ($\simeq$4155 cm^{-1}) is the Raman shift for the v = 0, j = 1 $\rightarrow$ v = 1, j = 1 transition of hydrogen. The presence of the stimulated Stokes scattering was verified by spectral analysis of the radiation leaving the cell.

The radiation leaving the high pressure cell was directed into a photoacoustic cell (PC) (previously described) containing pure hydrogen at 1 atm total pressure and then into a ballistic thermopile (T) where the energy was measured.

The two radiation fields drive an inverse Raman absorption process which populates the v = 1, j = 1 level. The subsequent collisional vibration-to-translation

relaxation process will then create a pressure wave which can be detected photoacoustically. A similar arrangement was used to probe the absorption region using thermal lensing (70).

If pure hydrogen at high pressure was used to generate the stimulated Stokes field, the frequency of the Stokes field would be pressure shifted (71) relative to the sample at a pressure of 1 atm and resonance could not be achieved. The addition of a calculated quantity of He induces a shift which compensates for the shift due to H_2-H_2 interactions (72).

In order to record the pressure wave the microphone output was fed into a variable gain amplifier (A) and then into an oscilloscope (O) where the trace, triggered when the laser fired, was photographed. Window absorption can constitute a significant source of noise when modulated excitation sources and phase sensitive detection is used because the noise will be synchronous with the desired signal. In a pulsed arrangement, however, a pressure wave due to window absorption will arrive at the microphone after the signal wave (having traveled a longer distance) thus allowing temporal discrimination.

There was, however, a catch. When the laser was fired the discharge of the capacitor bank generated electromagnetic interference (EMI) of sufficient intensity to

swamp any photoacoustic signal that might have been present. That the source of the problem was EMI was confirmed by the fact that essentially the same oscilloscope trace was obtained with radiation passing through the cell or blocked prior to reaching the cell.

Various remedies were attempted. Cables were shielded and special attention was given to grounding. The only effective reduction was obtained by moving the cell and detection electronics far away from the laser. Unfortunately, in moving the above, ruby laser power dropped below usable levels because of beam divergence.

The size of the ruby laser power supply precluded easily enclosing the capacitors and flashlamps in a so-called Faraday cage. The more compact layout of the Phase-R flash lamp pumped dye laser rendered such a project more feasible.

Because the output power of the Phase-R dye laser was about three orders of magnitude less than that of the ruby laser, it could not be substituted for the ruby laser in the above experiment. A new experimental approach was called for.

The easiest way to insure spatial and temporal coincidence when using a pulsed system is, as we have seen, to generate both fields with the same laser. To accomplish

this the laser was modified as shown in Figure 8. The rear total reflector was replaced with a Baush and Lomb grating (G_1) ruled at 600 grooves/mm with a first order Littrow blaze wavelength of 1·25 μm. By using the grating in second order (for maximum efficiency) in a Littrow configuration, the dye laser output could be tuned over the dye gain curve with a narrowed spectral width of about 15 cm^{-1} and little reduction in output power. The grooves of this grating, as indicated by Figure 8, are parallel to the plane of the diagram.

A second identical grating (G_2) was mounted about eight inches lateral to the axis of the laser with its grooves normal to the plane of the figure. A Glan laser prism (P) was mounted between the dye cavity (D) and the first grating (G_1) in such a manner that the dye fluorescence directed to each grating was polarized parallel to the grooves of the grating. This produced maximum lasing efficiency since at wavelengths below the blaze wavelength a grating will exhibit highest efficiency for radiation polarized parallel to the grooves.

The final product of the above modifications was in essence two dye lasers which shared a common dye cavity and output coupler. Each produced radiation of about 15 cm^{-1} spectral width and could be tuned over the gain curve of the dye used. Because of the orientation of the gratings

Figure 8. Dual grating dye laser configuration. Output mirror (M); Dye cavity (D); Glan prism (P); Grating (G).

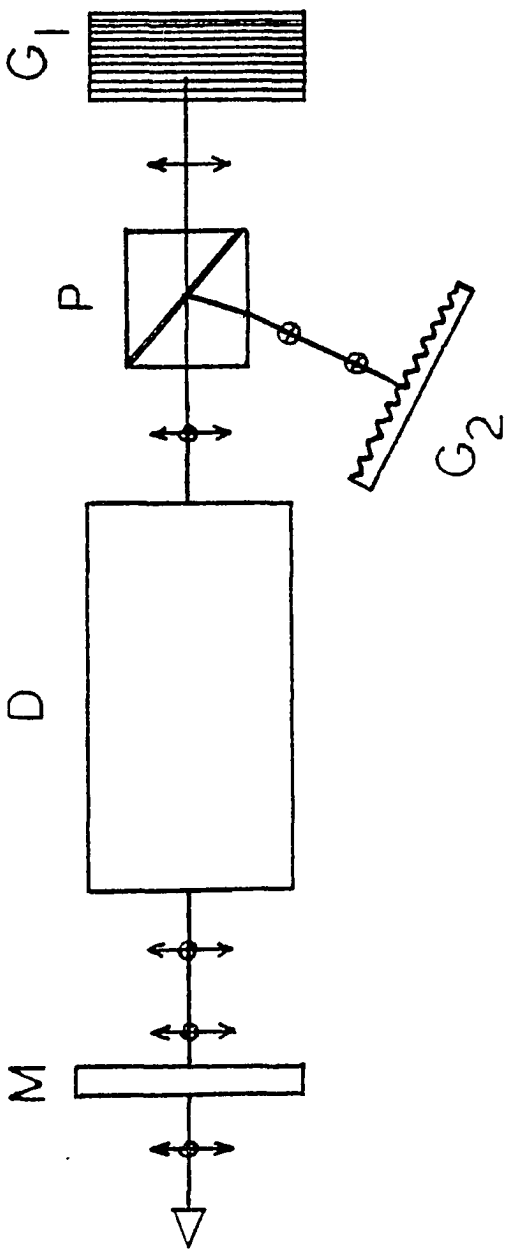
G1
P
G2
D
M

and the intracavity Glan prism, the two fields produced were polarized orthogonal to one another.

The above configuration offered the advantages of relatively high power for each of the two fields (up to about 50 kW/cm^2 unfocused) and guaranteed temporal and spatial coincidence. At the same time, however, the configuration imposed restrictions on the samples that could be studied. Because each field used the same dye as an active lasing medium, the sample chosen had to have a Raman shift which could be spanned by the gain curve of the dye. In practice this limited selection to those substances with shifts of less than about 300 cm^{-1}. This restriction, using small Raman shifts, imposed the additional handicap of reduced photo-acoustic signals since (equation 42) the pressure change is directly proportional to the Raman shift. Since the fields are polarized orthogonal to one another, only strongly depolarized Raman lines could be used. Because of the above restrictions, the 261 cm^{-1} line of chloroform was chosen for study using Rhodamine 6G dye.

With the gratings tuned to the 261 cm^{-1} resonance, the laser, including capacitors, was enclosed in 20 mesh copper screen which was then grounded.

A different photoacoustic cell featuring a reduced volume and using a Knowles Electronics BT1759 miniature

electret microphone was used. The microphone output was fed directly into a 7A22 differential amplifier on the Tektronix 7904 oscilloscope. In addition to providing a differential amplification mode, the amplifier offered a large DC offset and sensitivity up to 10 μV/div.

The copper screen cage appeared to have no discernible effect in suppressing the EMI. Again attention was given to shielding and grounding but without effect. A second cell was constructed which was nearly identical in size and material and the signal from the active cell measured differentially against it (the laser radiation did not pass through the second cell which functioned primarily as a reference antenna for the EMI). This arrangement resulted in a slight reduction in the EMI signal but not sufficient to allow the experiment to proceed. In addition the shot-to-shot variation in the EMI signal was on the order of several volts precluding the use of sensitive scales with DC offset. Once again significant EMI reduction could only be obtained by moving the cell so far away that laser irradiance dropped below usable levels.

It is clear from our experience that while photoacoustic detection using pulsed lasers is very attractive from a power standpoint, EMI poses a severe problem.

After reading a report of a successful pulsed photoacoustic experiment (73) (which made no mention of EMI problems), I decided to contact the author and learn his secret. It turned out to be quite straightforward. He simply bored a hole in the wall for the laser beam and placed the cell and detection electronics in the adjacent lab (74).

Even when an experiment fails, I believe in accentuating the positive. In this spirit I feel compelled to report that while the copper screen cage did not solve the EMI problem, it was highly effective in keeping flies off the laser optics.

Detection by Thermal Lensing

In 1964 Gordon et al. (75) reported the observation of long-lived buildup and decay transients in polar and nonpolar liquids when placed in the resonator cavity of a He/Ne laser. Time constants for the observed transients were on the order of a few seconds which suggested a thermal phenomenon. However, the strong localization of the phenomenon ruled out general heating effects. These authors proposed an explanation based on a thermally induced refractive index change in the liquids resulting from weak absorption of the laser radiation. They also suggested using the effect, known as thermal lensing or thermal blooming, as a sensitive means of measuring low absorbancies.

Since that time papers have appeared dealing with the theory of the effect (76-82), its application to absorption measurements (83-87), and recently its application to two-photon absorption spectroscopy (88-90).

Not all of the motivation for studying thermal lensing has resulted from its potential as a probe for weak absorption. Many researchers who use lasers know the effect as an unwanted complication in their work. When using lasers with high average powers, thermal lensing induced when the beam passes through windows or fluid cells may constitute a significant interference even when these materials are highly transparent. Thermal lensing may also be a source of distortion for high power beams in the atmosphere (80). The phase change resulting from the creation of the thermal lens can pose problems in phase-modulated or phase-locked systems. If the temperature coefficient of the refractive index (dn/dT) is positive, as it is in certain semiconductors and lead glasses, a converging lens will be thermally created leading to a self-focusing effect which may induce damage in the medium or precipitate the onset of unwanted non-linear phenomena.

The general principles underlying the formation of the thermal lens can readily be grasped. When a beam of radiation passes through a medium which possesses a finite absorption coefficient for the radiation, the absorbed energy

will be degraded into heat generating a localized increase in temperature. The increase in temperature will lead to a change in the local density and hence a change in the refractive index as can be seen from a first order expansion of the Lorentz-Lorenz law in terms of $\Delta\rho/\rho$ (82):

$$n^2 = n_0^2 + \{(n_0^2 - 1)(n_0^2 + 2)/3\}(\Delta\rho/\rho) \qquad (43)$$

where ρ and n_0 are the initial density and refractive index and n the refractive index resulting from a change, $\Delta\rho$, in the initial density. Equation 43 is valid for $(\Delta\rho/\rho) << 1$.

If the beam of radiation were of uniform irradiance about the axis propagation, the energy absorbed and the resulting change in refractive index would also be uniform. That such a beam would fail to induce a thermal lens by virtue of failing to create a radial refractive index gradient can be readily demonstrated mathematically (82).

The irradiance, I(r,t), of a laser beam as a function of the radial distance from the beam center, r(cm), and time, t, for the fundamental TEM_{00} mode can be written:

$$I(r,t) = \{2P(t)/\pi w^2\} \exp\{-2(r/w)^2\} \qquad (44)$$

where w(cm), the "beam radius", is the radius for which the field amplitude has fallen to e^{-1} of its axial value, and P(t) is the total power (watts) of the beam. It is reasonable to expect the variation in temperature, and

hence refractive index, to exhibit a similar functionality. Thus, if the beam irradiance is Gaussian, the optical absorption will lead to a temperature increase which is greatest along the axis of propagation and decreases radially. If dn/dt is negative, as it is for most media, the index of refraction will be lower on the axis than on the edges. Such a transverse index gradient will create a lens effect which will be divergent in nature thus leading to a blooming of the beam.

Most of the reported studies in which the thermal lensing effect was used to measure absorption coefficients have utilized an arrangement in which the output from a single cw laser, controlled by a shutter, served both as the pump source (to create the lens) and the probe beam (to monitor the blooming). A brief description of the theoretical approach used to describe the induced blooming will be instructive. The approach is that of Gordon et al. (76).

For simplicity the Gaussian nature of the lens is approximated by a parabolic function which can be viewed as a truncated expansion of the Gaussian form, i.e.:

$$n = n_o\{1 + \varepsilon(r/w)^2\} \tag{45}$$

A collimated ray entering parallel to the axis will be bent in a circular path the radius of curvature of which is (91):

$$R^{-1} = -\hat{r} \cdot \vec{\nabla} \log_e n = -2\varepsilon r/w^2 \qquad (46)$$

where $\hat{r}$ is a unit vector in the outward radial direction. If the cell length, ℓ, is small compared to the focal length, f, of the induced lens, a geometric construction readily gives:

$$f \simeq r/\Theta \simeq rR/\ell n_o = -(1/2\varepsilon)w^2/\ell n_o \qquad (47)$$

where Θ is the angle of divergence of the ray and n_o corrects for refraction of the rays leaving the cell. The first experiments of Gordon et al. (76) indicated a focal length of about 1 meter which together with $w = 0{\cdot}1$ cm and $\ell = 1$ cm gives $\varepsilon = 5 \times 10^{-5}$. For a typical liquid refractive index of 1·5, a total change in the refractive index from beam center to edge of only $7{\cdot}5 \times 10^{-5}$ would explain the observed effects. From:

$$n(r,t) = n_o + (dn/dT)\Delta T(r,t) \qquad (48)$$

and the fact that for many organic liquids of interest (86) $dn/dT \simeq -5 \times 10^{-4}/^{o}C$ one can deduce that a temperature change of about $0{\cdot}15\ ^{o}C$ will provide the necessary refractive index change.

When the heating effects from a Gaussian beam are treated in detail (76) it is found that the parabolic approximation holds fairly well up to r = w. Since most of the energy of the beam is encompassed in this radius (87%), the induced lens should exhibit little spherical aberration and the focal length derived from equation 45 should provide a very good approximation.

A detailed calculation of $\Delta T(r,t)$ in response to absorption from a cw Gaussian laser beam that is suddenly switched on and left on leads to an expression for the time development of the induced focal length (86).

$$f(t) = f_{\infty}(1 + t_c/2t) \tag{49a}$$

$$f_{\infty}(cm) = \pi Jkw^2/P\alpha\ell(dn/dT) \tag{49b}$$

$$t_c = w^2/4D \tag{49c}$$

where $k(cal/cm\text{-}sec\text{-}^{o}C)$ is the thermal conductivity, $P(watts)$ the power of the laser beam, $\alpha(cm^{-1})$ the absorption coefficient, $\ell(cm)$ the cell length, $D(cm^2/sec) = (k/\rho C_p)$ the thermal diffusivity ($\rho(g/cm^3)$ is the density and $C_p(cal/g\text{-}^{o}C)$ the specific heat), and J = 4·184 joules/cal.

Typical values of some of the above parameters for many organic liquids are: $k \simeq 3 \times 10^{-4}$ cal/cm-sec-^{o}C (76); $(dn/dT) \simeq -5 \times 10^{-4}/^{o}C$ (86); $D \simeq 10^{-3}$ cm^2/sec. The thermal

time constant, t_c, for beam radii (w) of about a millimeter will typically be on the order of a few seconds. For tightly focused beams, t_c can assume values on the order of microseconds (92).

From equations 49 one can see that the focal length of the induced lens changes from an initial (t = 0) value of infinity (no focusing) when the shutter is opened, to a steady state value of f_∞ determined by radial heat conduction. By measuring f_∞, the absorption coefficient can be obtained.

It will be instructive to examine qualitatively the factors contained in equations 49. The time required for the lens to form will depend on the thermal time constant, t_c. If the thermal diffusivity (D) is high, the rapid transfer of heat out of the lens region will lead to the rapid establishment of a steady state and its associated focal length, f_∞.

The smaller the value of the steady state focal length, the greater will be the observed defocusing. The factors which reduce the magnitude of f_∞ can readily be seen in equation 49b. A high irradiance, $P/\pi w^2$, will lead to strong defocusing by any, or all, of three possible mechanicsm: by providing a beam of high energy to the medium; by concentrating the beam energy in a very localized

region (small w); by providing the energy during a very short time interval. A low thermal conductivity (k) will allow a large thermal gradient to be established. A large absorption coefficient (α) will provide a large fraction of the radiant energy to be extracted as heat energy, and a large value of dn/dT will allow the temperature change to drive a large refractive index change. From equation 49b it can be seen that the nature of the induced lens (convergent or divergent) will be determined by the sign of dn/dT.

The development presented is valid for a radiation source which is suddenly switched on and left on for a period sufficiently long for the steady state focal length to be achieved. The same laser served as both pump and probe. Under such conditions there is a constant input of radiant energy into the system. If the radiant energy input is divided into very small intervals temporally, the response of the system during any of the intervals will depend not only upon the energy deposited during that interval but also upon the energy deposited and the system's response in each previous interval. The arrangement used in the study to be described used a cw laser as the probe and a pulsed laser as the pump source. When the lens is formed by an impulsive energy input, the response of the system during any interval after the laser

pulse will depend only on the energy deposited during that initial pulse. Thus, for a pulsed pump source, one can expect the evolution of the lens to be somewhat different.

It can be shown (88) that the lens induced by a one-photon absorption driven by a pulsed laser field is described by:

$$f(t) = f_o\{1 + 2t/t_c\}^2 \tag{50a}$$

$$f_o(cm) = kJ\pi w^4/8\ell D\alpha E(dn/dT) \tag{50b}$$

where E is the total energy (joules) in the pulse, t_c is given by equation 49c, and w is the radius of the pump beam in the sample.

By comparing equations 49 and 50 the difference in the evolution of the lenses resulting from cw and pulsed sources can be seen. The lens resulting from cw excitation, as we have seen, possesses an infinite focal length at $t = 0$ which changes progressively to lower values until reaching a minimum in the steady state ($t >> t_c$). Pulsed excitation, on the other hand, by in essence instantaneously (before the onset of heat loss from the absorption region) providing significant localized thermal energy to the medium, creates a lens the focal length which is a minimum at $t = 0$ and grows in value with time until ($t >> t_c$) it achieves an

infinite value when the density gradient is destroyed. Thus, a lens created by a pulsed source achieves maximum defocusing ability at $t = 0$ while one created by a cw source does so at $t = \infty$ ($t >> t_c$).

Experimentally the focal length is not measured. Hu and Whinnery (85) recognized that the more convenient extra-cavity cell arrangement provided good sensitivity by placing a converging lens between the laser and cell, locating the cell at the position of minimum radius of curvature of the beam wave front and, by using an aperture, monitoring the intensity at beam center. It can be shown (88) that maximum sensitivity is achieved when the cell is placed one confocal distant ($=\pi w_0^2/\lambda$, w_0 is the focused radius) before or after the probe beam focal point. If the cell is placed one confocal length before the focal point, the beam will be converging at that point and the thermal lens will tend to recollinate the beam. The effect at beam center in far field will be an increase in intensity as a result of the thermal blooming. If the cell is located a confocal length after the probe beam focal point, the beam will be diverging which will be enhanced by the thermal lens. The effect at beam center in far field will be a loss of intensity. For the latter arrangement, it can be shown (88):

$$(I_0 - I_m)/I_0 = -(5\cdot2)(dn/dT)\ell D\alpha\sigma_p E/kJw_0^2 \qquad (51)$$

where I_0 is the intensity of the unbloomed probe beam, I_m is the minimum intensity observed in the probe beam, and $\sigma_p(cm^{-1})$ is the energy of a photon in the pump beam.

The conditions that must be met for equation 51 to be valid are: The area sampled at beam center must be much smaller than the beam area; both pump and probe laser must be in the lowest fundamental mode (TEM_{00}); the absorption from the pump beam is sufficiently low that the fractional attenuation per unit length is constant in the sample; the distance from cell to detector must be less than the focal length but greater than the confocal length of the probe laser; the radius of the pump beam is constant over the length of the cell; ΔT must be sufficiently small that $n(r,t)$ can be accurately represented by a first order expansion in ΔT.

The first experiment to examine the feasibility of using the thermal lens effect to observe inverse Raman absorption could best be described as a highly qualitative study. Once again, as in an early photo-acoustic study, a single Ar^+ laser was available. The organic liquids which had been singled out for that photo-acoustic study (possessing Raman shifts equal to the difference between two of the Ar^+ laser lines) were resurrected and given one more chance to perform.

The broadband output from the Ar^+ laser was directed into a prism which served to disperse the individual lines. The lines, now spatially separated into individual beams were directed to a second prism oriented in such a manner that the diverging beams left the prism propagating parallel to one another. The separated parallel beams were then directed through two more prisms which recombined them once again. With the room darkened, the individual beams could readily be seen and identified. The spatially recombined beams were then focused into a cell containing the liquid of interest and then to a mirror which projected the combined beam on the wall about 8 meters away. Spatial mismatch of the beams could be detected by examining the far field image.

While the individual beams were spatially separated and parallel, all lines but the two spanning the Raman shift were blocked. The far field beam size was then determined. In order to see if there was any discernible resonance enhancement, one of the resonant lines was blocked and another non-resonant line unblocked and the power adjusted to keep the total input power approximately constant, or a single line used and the power again adjusted.

All of the liquids examined exhibited thermal lensing to some degree, but no resonant enhancement was observed.

It is quite clear in retrospect that the power levels used were simply inadequate to generate an inverse Raman absorption of sufficient magnitude to compete with the one-photon background absorption.

In order to provide the power levels required to generate a significant inverse Raman absorption (relative to the one-photon background absorption), it was necessary to use a high power pulsed source. For this reason, the dual grating dye laser described in the previous section and shown in Figure 8 was chosen.

The experimental arrangement used is shown schematically in Figure 9. The output from the dye laser (D) was focused with a 10 cm focal length lens (L_2) into a 10 cm sample cell (C). A microscope slide (B) functioning as a beam splitter directed a portion of the dye output to a ballistic thermopile (T). The output from the He/Ne probe laser was counter propagated into the sample cell after passing through a converging lens L_1). The He/Ne beam was focused about 20 cm before entering the cell and was thus diverging in the thermal lens region. After passing through the cell, a portion of the probe beam was split off and directed to a mirror (M) and then through a PTR model F103-C tunable grating filter (F) to an Amperex 56DVP photo-tube (P). The output from the photo-tube is

Figure 9. Experimental arrangement for thermal lensing study. He/Ne laser (HN); Lens (L); Sample cell (C); Beam splitter (B); Ballistic thermopile (T); Pulsed dye laser (D); Mirror (M); Filter (F); Photo-tube (P); Oscilloscope (O).

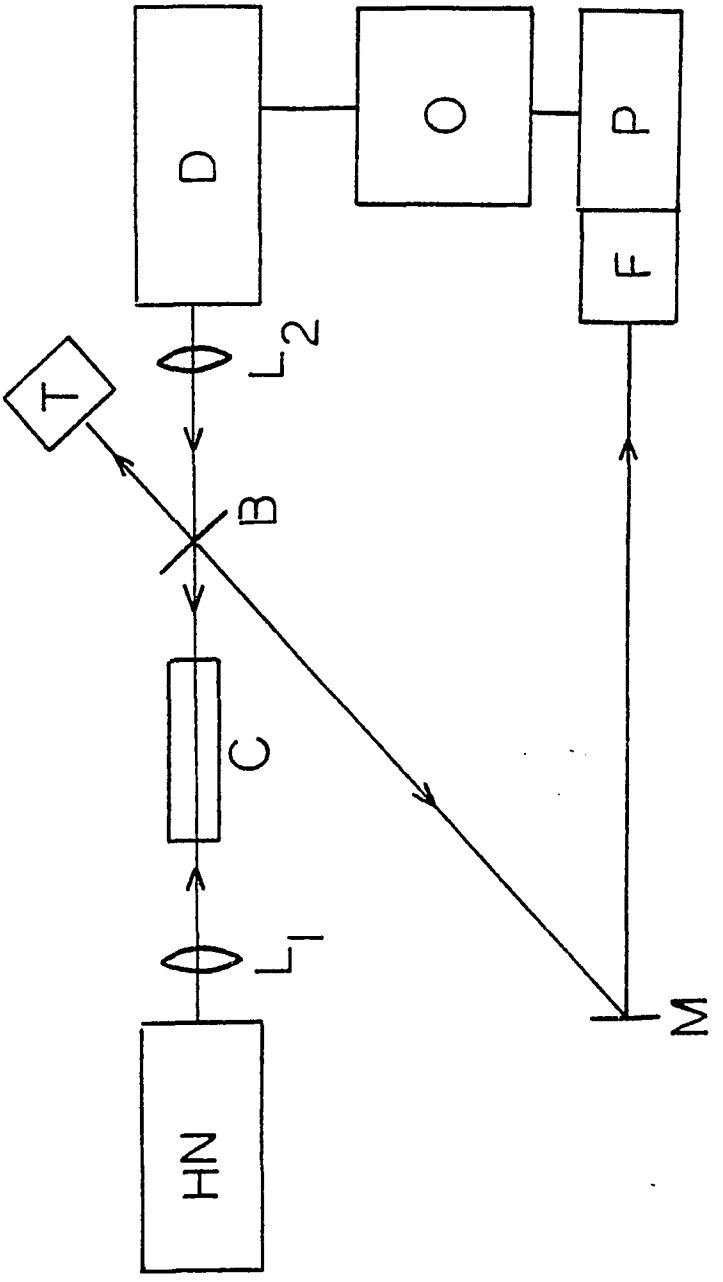
D
O
P
F
L_2
T
B
C
L_1
HN
M

then recorded on a Tektronix 7904 oscilloscope with a 7A22 vertical amplifier. The beam diameter at the filter was about 4 cm. The circular entrance aperture of the filter sampled an area at the beam center 2 mm in diameter.

The dual grating dye laser configuration possesses both advantages and disadvantages with respect to a thermal lensing study. The advantages are guaranteed spatial and temporal coincidence and tunability. The disadvantages are restriction to substances with strongly depolarized Raman lines and small Raman shifts, and only moderate high output power. In any caloric detection technique (photo-acoustic, thermal lensing) one desires to work with samples possessing large Raman shifts. The limitation of working with small shifts (that can be spanned by the dye gain curve of the dye) was therefore significant. In addition, small Raman shifts reduce the population factor δ (equation 10) in equation 16.

In order for the experiment to be feasible it would be necessary to generate an inverse Raman absorption which would enhance the one-photon lensing to a detectable degree. To estimate the enhancement we first examine equation 51. The ratio of the energy deposited by the inverse Raman absorption, U_R, and that deposited by the background one photon absorption, U_1, is:

$$U_R/U_1 = gE_R/\alpha E_1 \tag{52}$$

The inverse Raman absorption attenuates the excitation energy, E_L. However, the energy degraded into heat is not gE_L, but rather $gE_L\Delta\sigma_R/\sigma_L$. The one-photon absorption coefficient will attenuate both fields thus providing $\alpha(E_L + E_s)$ (since $\sigma_s \simeq \sigma_L$, it is assumed that α is the same for both) where E_s is the energy of the Stokes pulse. The gratings were tuned to give $E_L = E_s$. Therefore:

$$U_R/U_1 = g\Delta\sigma_R/2\alpha\sigma_L \tag{53}$$

To estimate g, the following values were used: $\sigma_L \simeq \sigma_s \simeq 15{,}625\ cm^{-1}$; $P_s \simeq 1\ MW/cm^2$; $N(d\sigma/d\Omega) \simeq 6{\cdot}5 \times 10^{-8}\ cm^2sr^{-1}$; $\Delta\sigma \simeq 15\ cm^{-1}$; $n_s \simeq 1{\cdot}5$; $\Delta\sigma_R = 262\ cm^{-1}$ (chloroform). The value of α at 633 nm, $1{\cdot}7 \times 10^{-5}$ (86), was used. Equation 53 yields an enhancement of 4%.

Two substances were singled out for the study, chloroform and bromoform. Chloroform had the advantages of a larger Raman shift ($262\ cm^{-1}$ vs. $153{\cdot}8\ cm^{-1}$) and a stronger Raman transition (93), but required working further out on the wings of the dye gain curve where power was reduced.

The active lasing medium was a 6×10^{-5} M solution of Rhodamine 640 (Exciton) dissolved in absolute ethanol. For maximum lasing efficiency, the dye temperature was maintained between 18 ^{o}C and 19 ^{o}C.

A preliminary study, using the ballistic thermopile, was undertaken to determine the output power/wavelength relationships for the dye. In order to prevent the gain at the wavelength of one of the gratings from parasitically reducing the gain of the other, it was necessary to choose the output wavelengths of the gratings so that, in addition to spanning the Raman shift, they fell at equal power points on the dye gain curve.

Figure 10A shows an oscilloscope trace of the reduction in intensity resulting from the thermal lensing effect in chloroform. The intensity increases from top to bottom while the time increases from left to right (0·2 msec/div). I_o represents the intensity of the unbloomed probe beam while I_m is the minimum intensity of the bloomed beam (at beam center). Reference to equations 50 will show that I_m corresponds to the intensity at $t = 0$ while I_o corresponds to the intensity at $t = \infty$ ($t >> t_c$). If the response time of the oscilloscope had been sufficiently fast, the rise to I_m on the trace would have been essentially vertical. The sigmoid shape of the rise is a result of an RC time constant of about 0·2 msec resulting from cable and amplifier capacitance and resistance. If the trace time was sufficiently long, the intensity would drop (on the trace) from a low of I_m back to the unbloomed intensity. Since the experiment was designed to determine

Figure 10. Oscilloscope traces showing: (A) Reduction in He/Ne laser intensity resulting from thermal lensing; (B) Increase in Ar^+ laser intensity resulting from polarization rotation.

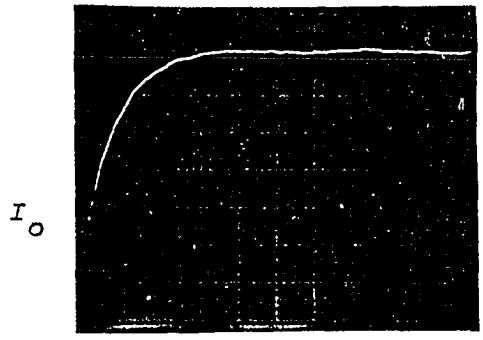

A

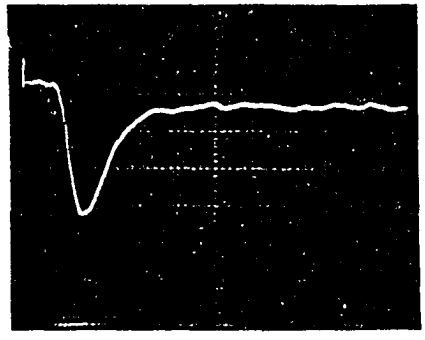

B

the absorption enhancement due to inverse Raman absorption and not the temporal behavior of the lens, only $(I_o - I_m)$ and I_o were determined (see equation 51). The value of I_o (volts) was determined by monitoring the DC response of the photo-tube to the unbloomed beam. To measure a small $(I_o - I_m)$, a DC offset was introduced to the trace. For the trace shown, $I_o = 60V$ and $(I_o - I_m) \simeq 2{\cdot}25V$ (0·5V/div). Using equation 51 with $W_o \simeq 1$ mm; $E \simeq 60$ mJ, $\sigma_p \simeq 15625$ cm^{-1}, $dn/dT = 5{\cdot}8 \times 10^{-4}\ {}^oC^{-1}$, $D \simeq 7\ 8 \times 10^{-4}$, $k \simeq 2{\cdot}7 \times 10^{-4}$, and $\ell = 10$ cm, one calculates $\alpha \simeq 1{\cdot}9 \times 10^{-5}$ which is to be compared to the literature value (86) for the one photon absorption coefficient in this region of $1{\cdot}7 \times 10^{-5}$.

No enhancement could be observed as the grating for the excitation field was tuned through resonance for either chloroform or bromoform. The system and detection scheme, it appears, was incapable of detecting an enhancement of only 4%.

The experimental arrangement used in this study possessed several severe shortcomings. The gratings provided output with a spectral width of about 15 cm^{-1}, a rather broad width. If the dye laser spectral width could be reduced, without significant power reduction, so that the width of Raman line became the limiting width,

the enhancement could be increased typically by a factor of 6 or 7.

The multimode nature of the dye laser output could render quantitation difficult since the pertinent equations are valid for the TEM_{00} mode. An aperture could be used to select this mode but at the price of power. For this reason, a high power pulsed laser, e.g., a ruby laser, which could provide high power in the fundamental mode would be advantageous. However, a more complex experimental arrangement would probably be necessary compared to this arrangement where a single laser provides both the fields necessary for the inverse Raman absorption. It should also be kept in mind that, even in seemingly transparent liquids, a non-zero background one-photon absorption coefficient (that appears to be the result of vibrational transitions involving higher harmonics (94)) will exist at the excitation and Stokes frequencies. As higher and higher powers are provided to the system to generate a significant inverse Raman absorption coefficient, the total absorbed power may lead to violations underlying the equations used to quantitate the thermal lens effect (e.g., generate a $\Delta T(r,t)$ so large that equation 48 no longer accurately describes $n(r,t)$).

An accurate means of measuring the Stokes power must be available which means accurately measuring both the

Stokes energy and the pulse width. The pulse width was not monitored on a shot-to-shot basis. Previous studies showed it to be 1 μsec to a high degree of reliability. The energy provided by the thermopile generated a signal of about 1 μV. Fluctuations at that level of sensitivity could provide significant error. To insure that only the Stokes energy reaches the detector, the beam splitter should be oriented at Brewster's angle relative to the excitation field.

The restriction to strongly depolarized lines and, especially, to small Raman shifts posed a severe restriction especially in light of the fact that the technique is caloric in nature.

Detection by Polarization Rotation

When an inverse Raman event takes place in a medium, the most obvious consequence is an attenuation of the excitation field. By measuring the attenuation, the inverse Raman absorption coefficient can be calculated. However, if the attenuation is small, it is necessary to measure a small difference between two large signals. The magnitude of fluctuations of the two fields, although small compared to the magnitude of the fields, may nevertheless be large compared to the difference between them and therefore a large uncertainty can exist in the absorption measurement.

A less obvious consequence of an inverse Raman event is the possibility of altering the polarization of the excitation field. To see how this is possible we allow a polarization mismatch to exist between the excitation and Stokes fields (both of which we take to be linearly polarized). We let the Stokes polarization direction define the coordinate system and decompose the excitation field into its components parallel and orthogonal to the Stokes polarization direction. For simplicity, the Raman transition is taken to be polarized. Inverse Raman absorption will take place only from the component of the excitation field parallel to the Stokes field. The result will be not only a net absorption from the resultant excitation field but also a rotation of the polarization vector. The extent of the rotation will depend upon the magnitude of the absorption, the polarization mismatch, and the depolarization ratio of the transition (see Appendix C).

The fields need not be restricted to linear polarization. If the excitation field (the probe field) is linearly polarized and the Stokes field (the pump field) is circularly polarized, a decomposition of the probe field into its circular components and an argument similar to the above will reveal that the inverse Raman absorption will lead to an elliptically polarized probe beam during the interaction time.

Many reports of experiments using polarization rotation detection have appeared in the literature (94-100). The technique reported here is essentially that of Heiman et al. (101), which they call the Raman induced Kerr effect (RIKE).

The experimental arrangement used to generate and detect the polarization rotation is shown in Figure 11. An Ar^+ laser (A) operated in a cw single line mode provided the probe (excitation) field. The probe field was directed through a half-wave plate which rotated the linear polarization vector (initially perpendicular to the plane of the figure) through an angle of 45^o. After reflecting off mirrors M_1 and M_2, the beam passed through a polarizer (P_1) which was oriented to pass the maximum probe intensity. This polarizer served to enhance the polarization purity of the probe beam. After passing through the sample cell (C), the probe beam was directed through a second polarizer (P_2), into a PTR model F103-C tunable grating filter (F) for scattered light rejection and then into an Amperex 56DVP photo-tube (PT). The photo-tube output was displayed on a Tektronix 7904 oscilloscope with a 7A22 vertical amplifier. The pump (Stokes) field was provided by a Phase-R model D-2100 flash lamp pumped dye laser (D) operated in a single grating configuration. The output from the dye laser, linearly polarized

Figure 11. Experimental arrangement for polarization rotation study. Dye laser (D); Mirror (M); Beam reducer (BR); Sample cell (C); Polarizer (P); Half wave plate (H); Ar^+ laser (A); Filter (F); Photo-tube (PT); Oscilloscope (O).

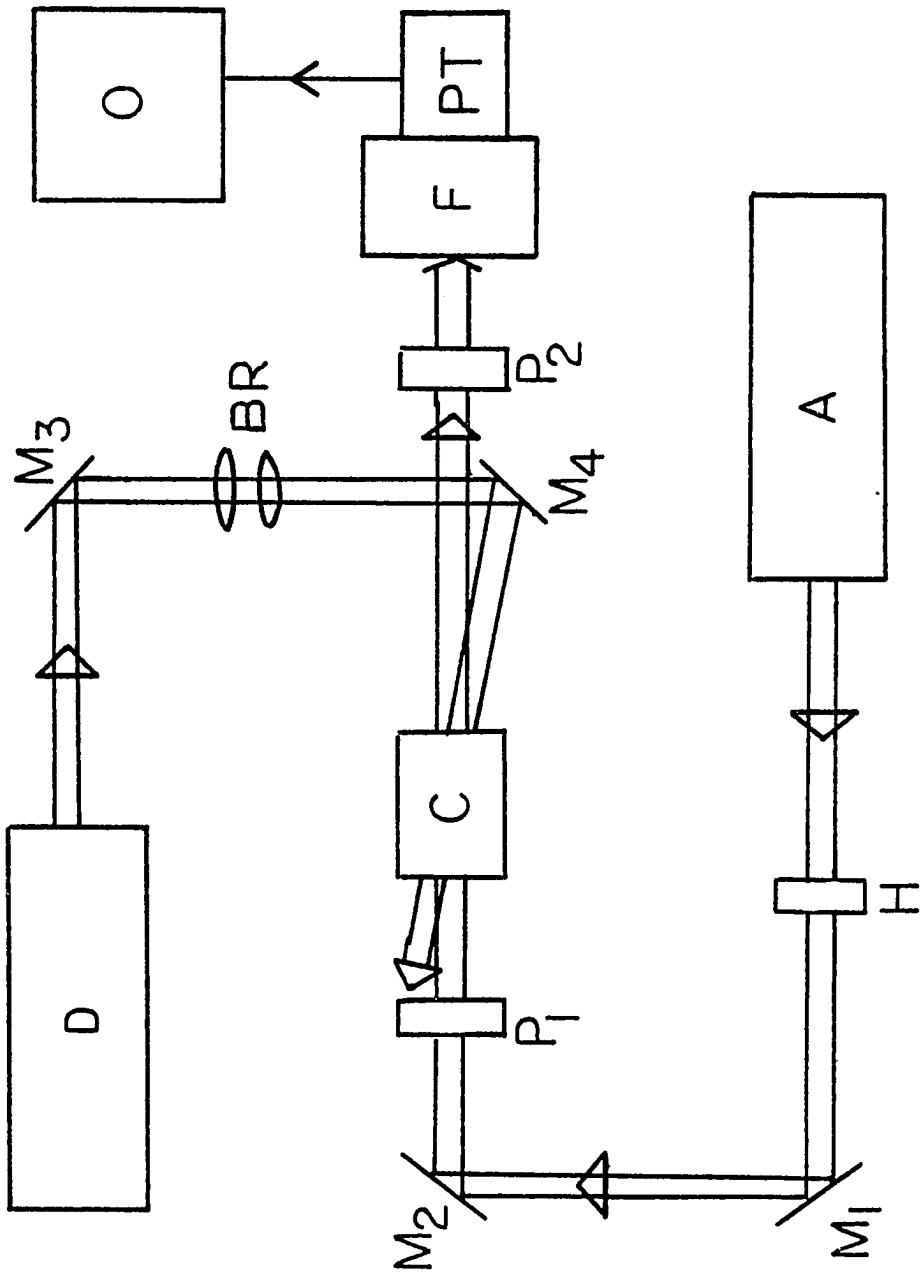
O
PT
F
A
P_2
BR
M_3
M_4
C
H
D
P_1
M_2
M_1

perpendicular to the plane of the figure, was directed via mirror M_3 into a beam reducer (BR), then into the sample cell via mirror M_4. Mirror M_4 was placed as close to the probe beam as possible without interrupting it. This configuration was designed to allow the pump and probe beams to cross at as shallow an angle as possible in the sample cell. The crossing angle was estimated to be no more than 2^{o}. Although not shown in Figure 11, a ballistic thermopile was used to measure the energy of the pump beam exciting the cell. The insure spatial overlap of the two beams an aluminum disk with a 3 mm aperture was placed in the middle of the sample cell and both beams made to pass through it.

After alignment of the filter and phototube, polarizer P_2 was adjusted until the minimum probe beam intensity was passed. Ideally no radiation should have passed through the second polarizer when crossed with respect to the first. However, any optical element placed in the path of the probe beam between the first and second polarizer introduced some depolarization which allowed radiation to reach the phototube and produced a non-zero background. This is one reason why the probe and pump beams were crossed in the interaction region and not propagated co-linearly which would have required the introduction of an additional optical element in the probe beam path. The major source of background radiation was a result of the depolarization induced by

the cell windows. To minimize this depolarization, the thinnest available microscope slide cover slips (number 1) were used. They were carefully examined for optical defects and then carefully mounted using a silicon cement which provided a flexible seal to reduce strain. It was very important that the cell windows be as parallel as possible not only to reduce depolarization effects but alos to reduce alignment problems resulting from refraction as the probe beam left the sample cell.

The laser dye with the highest output power available in our laboratory at the time of this study was Rhodamine 6G. A 6×10^{-5} M solution of this dye in methanol provided usable output from about 573 to 600 nm. A search was therefore conducted for substances with Raman transitions in the vicinity of 3000 cm^{-1}. Several substances were rejected because self-thermal blooming of the probe beam led to too high a background level. Finally, three substances were chosen for study, acetonitrile (CH_3CN), benzene, and water.

It can be shown (see Appendix C) that for a polarization mismatch of 45^{o}, the intensity passing through the second polarizer, I_L', as a result of the inverse Raman absorption is:

$$I_L' = I_L(0)\{g\ell/4\}^2 \tag{54}$$

where $I_L(0)$ is the probe beam intensity entering the sample cell. In order to interpret the observed signals, a normalized signal was obtained by dividing the peak signal (mV) by $I_L(0)$ and $\{P_s\}^2$. Such a procedure is valid if the phototube gain is the same for all spectra, and if the variation in σ_s^8 is negligible across the scan.

Figure 10B shows a typical oscilloscope trace of the result of the polarization rotation. The horizontal axis represents time (0·5 μsec/div) and increases left to right. The vertical axis represents intensity passing through the second polarizer and increases top to bottom. Initially the trace is flat representing the background intensity passing through the polarizer. Coincident with the arrival of the pump pulse the intensity increases and reproduces, temporally, the profile of pump pulse. If the dye laser is blocked, no such dip is observed. If the Ar^+ beam is blocked, a flat trace also results indicating an absence of reflected light from the pump beam.

Benzene exhibits a strong transition at about 3065 cm^{-1}. Using the 496·6 nm line from the Ar^+ laser as the probe source, the dye laser was scanned through the resonance region. A very large signal (10 to 15 times greater than that seen with any other substance) was observed at the resonance shift. Although the signal rapidly dropped

off about the resonance position, small signals could be detected off resonance.

Acetonitrile exhibits a very strong Raman transition with a shift of 2942 cm^{-1} and an adjacent strong transition at 2999 cm^{-1} (67, 93). Using the 496·6 nm Ar^+ line, the probe beam was oriented 45° relative to the pump beam and the resonance region scanned by adjusting the dye laser grating. The region scanned covered about 100 cm^{-1} and included both Raman transitions.

Acetonitrile provided a signal across the spectral region scanned. The maximum signal spanned a region of about 40 cm^{-1} which, considering the spectral width of the pump field ($\simeq$ 15 cm^{-1}), is not inconsistent with published spectra (67).

When the Ar^+ laser was tuned off resonance to the 514·5 nm line, a reduced signal ($\simeq$ 20% of the resonant signal) was observed. However, tuning off resonance by using the 488 nm Ar^+ line provided signals on the order of the resonance signals.

When the resonant 496·6 nm line was used polarized parallel to the pump field, spectral signals approximately 20-80% of the resonant signals were observed.

Conventional Raman spectra show that water possesses a broad Raman line with a relatively flat peak the shift of which runs from about 3250 cm^{-1} to 3400 cm^{-1}. Using

the 488 nm Ar^+ line as the probe beam, the resonance region was scanned. A broad spectral profile consistent with the Raman profile was obtained. When the off resonance 514·5 nm Ar^+ line was substituted, however, signals on the order of the resonance signals were observed but were of sufficient uniformity that the region appeared featureless. Significant signals were obtained on resonance using the 496·5 nm Ar^+ line which dropped in magnitude as one tuned away from resonance producing a profile similar to that obtained using the resonant 488 nm line.

Clearly the processes taking place in the sample of interest which lead to depolarization are complex. It is well known (102) that the presence of an intense electric field (e.g., the focused pump beam) will induce a non-linear polarization which will generate an anisotropy in the refractive index the medium presents to a second field (e.g., the probe field) in the medium. This effect, the optical Kerr effect, will, in the experiments described, lead to an off-resonance depolarization. The optical Kerr effect can be eliminated by using a circularly polarized pump field. In addition, as one tunes away from resonance, the induced refractive index will change rapidly in the near resonance regime (using a linearly polarized pump beam), reach its maximum (or minimum), then approach

its far off-resonance value. Thus, the depolarization resulting from this non-linear dispersion may distort lineshapes and produce significant off (but near) resonance values as were observed in this study.

In addition, the thermal lens effect introduces uncertainty into the observed signals. The lens effect may depolarize directly or may lead to increased intensity passed by the polarizer because the diverging rays are not rejected efficiently. Whatever the effect, it promises to be difficult to quantitate.

Of the substances studied, water would have provided a relatively interference free system. A previous study of the optical Kerr effect using a ruby laser failed to detect such an effect in water (103) (it is possible, however, that the proximity to a Raman transition in this study significantly enhanced the effect). From the standpoint of density and specific heat, water is a relatively poor thermal lens medium (although the one-photon absorption coefficient in this region may be large and a significant lensing effect may be possible). The absence, in this study, of a signal from water when the probe and pump beams were polarized parallel to one another tends to confirm the belief that the thermal lens effect probably played a subordinate role in contributing to the observed off resonance signals.

On the other hand, the two organic species studied, on the basis of density and heat capacity, are more efficient media for the creation of a thermal lens (if one-photon absorption coefficients are comparable). The optical Kerr effect has been demonstrated in benzene (103) while acetonitrile was not included among other organics in which the effect has been studied (104).

No attempt was made to extract quantitative information from the observed signals because of the obvious complexity introduced by the use of a linearly polarized pump beam. The use of a circularly polarized probe will allow thermal lens effects to be separated from optical Kerr effects.

Conclusions

The studies reported in this chapter were undertaken to examine the feasibility of applying the described detection techniques to the inverse Raman effect. In summary, the following conclusions are offered.

Of the three techniques studied, photo-acoustic detection appears to hold the most promise as a probe for inverse Raman absorption. Obviously this conclusion is not based heavily on photo-acoustic experiments reported herein, but rather on the successes reported in the literature (31, 32, 66). Photo-acoustic detection can offer high sensitivity

by providing a signal against a very low background. Phase sensitive detection can further enhance the sensitivity. By using modulation schemes which do not interrupt the power input to the cell (e.g., by modulating the polarization or wavelength of the field, or through the Stark or Zeeman effects modulating the resonance frequency) resonant background interference from window absorption or scattering can be eliminated. Reports of the successful use of pulsed lasers (66, 73, 105) indicates that the EMI problem can be controlled. Since the photo-acoustic effect is a caloric effect, the study of small Raman shifts will pose problems. However, for the most part, it appears that photo-acoustic detection presents problems which are technical not fundamental.

Polarization rotation detection, like photo-acoustic detection, offers, in principal, signals against a very low (ideally zero) background. Unlike photo-acoustic detection, however, the study of small Raman shifts presents no fundamental problem except the need for good spectral filtering of scattered light. The primary problem confronting the use of polarization rotation is the ubiquitous presence of thermal lensing which can generate a background interference that is difficult to quantitate, and can introduce uncertainty in the size of the beams in

the interaction region. In addition, it appears that the use of a circularly polarized pump beam is necessary for the generation of unambiguous spectra.

The use of the thermal lens effect to probe inverse Raman absorption poses several fundamental problems. The lensing effect due to the inverse Raman absorption must be detected as an enhancement relative to the background one-photon lensing. Increasing the Stokes power to generate an inverse Raman absorption coefficient of sufficient size to compete with the one-photon absorption coefficient will also increase the one-photon background effect. However, power must not be increased to levels where assumptions underlying the equations describing the formation of the lens are no longer valid. Quantitative studies will require the determination of the one-photon absorption coefficients at both Stokes and excitation frequencies. In addition, the defocusing effect may render it difficult to accurately determine power densities in the interaction region thus injecting additional uncertainty into the quantitative treatment of data. Because three fields are necessary (two to generate the lens, one to probe the lens), the experimental configurations may prove less straightforward than other techniques.

REFERENCES

1. Shore, B. W. Am. J. Phys. 1979, 47(3), 262.

2. Peticolas, W. L. Ann. Rev. Phys. Chem., 1967, 18, 233.

3. Bloembergen, N. Am. J. Phys., 1967, 35(11), 989.

4. Buckingham, A. D. J. Chem. Phys., 1965, 43(1), 25.

5. Jones, W. J.; Stoicheff, B. P. Phys. Rev. Lett., 1964, 13(22), 657.

6. McLaren, R. A.; Stoicheff, B. P. Appl. Phys. Lett., 1970, 16(3), 140.

7. Alfano, R. R.; Shapiro, S. L. Chem. Phys. Lett., 1971, 8(6), 631.

8. Duardo, J. A.; Johnson, F. M.; El-Sayed, M. A. Phys. Lett., 1966, 21(2), 168.

9. Tsunoda, Y. Jap. J. Appl. Phys., 1972, 11(9), 1293.

10. Gadow, P.; Lau, L.; Thuy, Ch. T.; Weigmann, H. S.; Werncke, W.; Lenz, K.; Pfeiffer, M. Optics Comm., 1971, 4(3), 226.

11. Yeung, E. S. J. Molec. Spectrosc., 1974, 53, 379.

12. Morris, M. D.; Wallan, D. J.; Ritz, G. P.; Haushalter, J. P. Anal. Chem., 1978, 50(13), 1796.

13. Hughes, L. J.; Steenhoek, L. E.; Yeung, E. S. Chem. Phys. Lett., 1978, 58(3), 413.

14. Long, D. A. "Raman Spectroscopy," McGraw-Hill: New York, 1977.

15. MacQuillan, A. K.; Stoicheff, B. P. In "Physics of Quantum Electronics," P. Kelly et al. Eds., McGraw-Hill: New York, 1966; p. 192.

16. Long, D. A. In "Advances in Raman Spectroscopy," Vol. 1, J. Mathieu Ed., Heyden: London, 1973.

17. Placzek, G., Handbuch der Radiologie, 1934, 6(2), 205.

18. Fenner, W. R.; Hyatt, H. A.; Kellam, J. M.; Porto, S. P. S. J. Opt. Soc. Am., 1973, 63(1), 73.

19. Yariv, A. "Quantum Electronics," 2nd ed. Wiley: New York, 1975.

20. Pantell, R. H.; Puthoff, H. E. "Fundamentals of Quantum Electronics," Wiley: New York, 1969.

21. Hellwarth, R. W. Appl. Opt., 1963, 2(8), 847.

22. Owyoung, A.; Jones, E. D. Opt. Lett., 1977, 1, 152.

23. Maier, M. Appl. Phys., 1976, 11, 209.

24. Werncke, W.; Lau, A.; Pfeiffer, M.; Weigmann, H. J.; Hunsalz, G.; Lenz, K. Opt. Comm., 1976, 16(1), 128.

25. Strizhevskii, V. L.; Kondilenko, E. I. Optics and Spectry., 1970, 30, 127.

26. Dowley, M. W.; Eisenthal, K. B.; Peticolas, W. L. Phys. Rev. Lett., 1967, 18, 531.

27. Behringer, J. In "Chemical Society Specialist Periodical Reports, No. 29, Molecular Spectroscopy, Vol. 2," D. A. Long et al. Eds., Chemical Society: London, 1974.

28. Lin, S. H.; Reid, E. S.; Tredwell, C. J. Chem. Phys. Lett., 1974, 29, 389.

29. Von Holle, W. U. S. Ballistic Research Laboratories Memorandum Report, No. 2607, 1974.

30. Kneipp, K.; Werncke, W.; Ponath, H. E.; Klein, J.; Lau, A.; Thuy, C. D. Phys. Stat. Sol. (B), 1974, 64, 589.

31. Barrett, J. J.; Berry, M. J. Appl. Phys. Lett., 1979, 34, 144.

32. Patel, C. K. N.; Tam, A. C. Appl. Phys. Lett., 1979, 34, 760.

33. Sushchinskii, M. M. "Raman Spectra of Molecules and Crystals," Israel Program for Scientific Translations Ltd.: New York, 1972.

34. Hirschfeld, T.; Schildkraut, E. R.; Tannebaum, H.; Tanenbaum, D. Appl. Phys. Lett., 1973, 22, 38.

35. Regnier, P. R.; Taran, J. P. E. Appl. Phys. Lett., 1973, 23, 240.

36. McClung, F. J.; Weiner, D. J. Opt. Soc. Am., 1964, 54, 641.

37. Lotem, H.; Araujo, B. D. Phys. Rev., 1977, B16, 1711.

38. Stansbury, E. J.; Crawford, M. F.; Welsh, H. L. Can. J. Phys., 1953, 31, 954.

39. Bernstein, H. J.; Allen, G. S. Opt. Soc. Am., 1955, 45, 237.

40. Brandmuller, J.; Schrotter, H. W. Z. Phys., 1957, 149, 131.

41. Yoshino, T.; Bernstein, H. J. J. Mol. Spectrosc., 1958, 2, 213.

42. Yoshino, T.; Bernstein, H. J. J. Mol. Spectrosc., 1958, 2, 241.

43. Golden, D. M.; Crawford, B. J. Chem. Phys., 1962, 36, 1654.

44. Hyatt, H. A.; Cherlow, J. M.; Fenner, W. R.; Porto, S. P. S. J. Opt. Soc. Am., 1973, 63, 1604.

45. Kolos, W.; Wolniewicz, L. J. Chem. Phys., 1967, 46, 1426.

46. Ford, A. L.; Browne, J. C. Phys. Rev., 1973, A2, 418.

47. Bridge, N. J.; Buckingham, A. D. J. Chem. Phys., 1964, 40, 2733.

48. Rowell, R. L.; Aval, G. M.; Barrett, J. J. J. Chem. Phys., 1971, 54, 1960.

49. Kobayasi, T.; Inaba, H. Appl. Phys. Lett., 1970, 17, 139.

50. Schrotter, H. W.; Klockner, H. W. In "Raman Spectroscopy of Gases and Liquids," A. Weber Ed., Springer-Verlag: New York, 1979.

51. Fouche, D. G.; Chang, R. K. Appl. Phys. Lett., 1971, 18, 579.

52. Fouche, D. G.; Chang, R. K. Appl. Phys. Lett., 1972, 20, 256.

53. Penney, C. M.; Goldman, L. M.; Lapp, M. Nature Phys. Sci., 1972, 235, 110.

54. Eckhardt, G.; Wagner, W. G. J. Mol. Spectrosc., 1966, 19, 407.

55. Sidorov, N. K.; Stalmakhova, L. S.; Bogachyov, N. V. Opt. Spectrosc., 1971, 30, 375.

56. Skinner, J. G.; Nilsen, W. G. J. Opt. Soc. Am., 1968, 58, 113.

57. Kato, Y.; Takuma, H. J. Opt. Soc. Am., 1971, 61, 347.

58. Kato, Y.; Takuma, H. J. Chem. Phys., 1971, 54, 5398.

59. Swofford, R. L. Ph.D. Thesis, Univ. of California (Berkeley), 1973.

60. Owyoung, A.; Peercy, P. S. J. Appl. Phys., 1977, 48, 674.

61. Zeiger, H. J.; Tannewald, P. E.; Kern, S.; Herendeen, R. Phys. Rev. Lett., 1973, 11, 419.

62. Bell, A. G. Am. J. Sci., 1880, 20, 305.

63. Kerr, E. L.; Atwood, J. G. Appl. Opt., 1968, 7, 915.

64. Rosenewaig, A. Science, 1973, 181, 657.

65. Patel, C. K. N.; Tam, A. C. Chem. Phys. Lett., 1979, 62, 511.

66. West, G. A.; Siebert, D. R.; Barrett, J. J. J. Chem. Phys., in press.

67. Dollish, F. R. "Characteristic Raman Frequencies of Organic Compounds," Wiley: New York, 1974.

68. Bhagavantam, S.; Rao, A. V. Nature, 1937, 139, 114.

69. Minck, R. W.; Terhune, R. W.; Rado, W. G. Appl. Phys. Lett., 1963, 3, 181.

70. Ducuing, J.; Joffrin, C.; Coffinet, J. P. Opt. Comm., 1970, 2, 245.

71. May, A. D.; Varghese, G.; Stryland, J. C.; Welch, H. L. Can. J. Phys., 1964, 42, 1058.

72. Lallemand, P.; Simova, P. J. Molec. Spectrosc., 1968, 26, 262.

73. Cox, D. M. Opt. Comm., 1978, 24, 336.

74. Cox, D. M. EXXON, Linden, N.J., Private communication.

75. Gordon, J. P.; Leite, R. C. C.; Moore, R. S.; Porto, S. P. S.; Whinnery, J. R. Bull. Am. Phys. Soc. Ser., 1964, 9, 501.

76. Gordon, J. P.; Leite, R. C. C.; Moore, R. S.; Porto, S. P. S. J. Appl. Phys., 1965, 36, 3.

77. Carman, R. L.; Kelley, P. L. Appl. Phys. Lett., 1968, 12, 241.

78. Aitken, A. H.; Hayes, J. N.; Ulrich, P. B. Appl. Opt., 1973, 12, 193.

79. Kleiman, H.; O'Neil, R. W. Appl. Phys. Lett., 1973, 23, 43.

80. Ulrich, P. B.; Wallace, J. J. Opt. Soc. Am., 1973, 63, 8.

81. Buser, R. G.; Rohde, R. S. Appl. Opt., 1975, 14, 50.

82. Hayes, J. N. Appl. Opt., 1972, 11, 455.

83. Solimini, D. J. Appl. Phys., 1966, 37, 3314.

84. Leite, R. C. C.; Moore, R. S.; Whinnery, J. R. Appl. Phys. Lett., 1964, 5, 141.

85. Hu, C.; Whinnery, J. R. Appl. Opt., 1973, 12, 72.

86. Whinnery, J. R. Acc. Chem. Res., 1974, 7, 225.

87. Dovichi, N. J.; Harris, J. M. Anal. Chem., 1979, 51, 728.

88. Twarowski, A. J.; Kliger, D. S. Chem. Phys., 1977, 20, 253.

89. Twarowski, A. J.; Kliger, D. S. Chem. Phys., 1977, 20, 259.

90. Twarowski, A. J.; Kliger, D. S. Chem. Phys. Lett., 1977, 50, 36.

91. Born, M.; Wolf, E. "Principle of Optics," 4th ed., Pergamon: New York, 1975.

92. Dabby, F. W.; Boyko, R. W.; Shank, C. V.; Whinnery, J. R. IEEE J. Quantum Electron., 1969, 5, 516.

93. Herzberg, G. "Infrared and Raman Spectra of Polyatomic Molecules," Van Nostrand Reinhold: New York, 1945.

94. Owyoung, A. IEEE J. Quantum Electron., 1978, 14, 192.

95. Liao, P. F.; Bjorklund, G. C. Phys. Rev. Lett., 1976, 36, 584.

96. Chebotayev, V. P.; Troshin, B. I. Appl. Phys., 1976, 11, 303.

97. Teets, R.; Feinberg, R.; Hänsch, T. W.; Schawlow, A. L. Phys. Rev. Lett., 1976, 37, 683.

98. Shalagin, A. M. Sov. Phys. JETP, 1978, 46, 50.

99. Song, J. J.; Lee, J. H.; Levenson, M. D. Phys. Rev., 1978, A17, 1439.

100. Adonts, G. G.; Kocharyan, L. M. Opt. Spectrosc., 1976, 40, 410.

101. Heiman, D.; Hellwarth, R. W.; Levenson, M. D.; Martin, G. Phys. Rev. Lett., 1976, 36, 189.

102. Maker, P. D.; Terhune, R. W. Phys. Rev., 1965, 137, A801.

103. Mayer, G.; Gires, F. C. R. Acad. Sc. Paris, 1964, 258, 2039.

104. Giuliani, J. F.; Van Laak, J. J. Opt. Soc. Am., 1976, 66, 372.

105. Aoki, T.; Katayama, M. Jap. J. Appl. Phys., 1971, 10, 1303.

ACKNOWLEDGMENTS

A wise man once noted that the only difference between graduate school and hell is that in hell you don't have to write quarterly reports. I know he was a wise man because shortly thereafter he left graduate school for medical school to become someday, perhaps, a famous gynecologist like his friend Cristiano.

While I do in some small measure agree with his sentiments (it is disappointing to spend years studying in order to receive the title of doctor only to find that the local pharmacy will not honor your prescriptions), graduate school is not without its rewards. It offers the opportunity to grow as a scientist and to grow as an individual, to learn about the universe and to learn about one's self, and, perhaps, to make some small contribution to man's understanding of the universe around him. How, you may ask, can I indulge in such shameless hyperbole? Perhaps it is because habits acquired while writing a thesis have a finite half life.

The purpose of this section is to acknowledge the aid and support I have received from many individuals during my passage through graduate school. If a name or two is omitted it is only because those individuals have come up with enough money to keep their names out of this thesis.

The contributions of the following individuals, the naive, the daring, and those whose checks came back marked "insufficient funds", are thus noted. To crazy Dave my thanks for being a fellow traveler in craziness; to Larry, the group's answer to Dr. Doolittle, (he talked to the instruments, as did we all, but to him the instruments listened), my thanks for the technical assistance; to Mike, whose unfailing willingness to accompany anyone to the local watering holes allowed him to preside over the destruction of an estimated $7{\cdot}2 \times 10^{12}$ liver cells, my thanks for confirming the presence of the insanity around us; to Cris, who was told he would rub shoulders with some of America's finest chemists at ISU and found it to be true only because the contractors placed the urinals so close together, I offer my thanks for being shorter than I, and my best wishes for success in his quest for the ideal woman (beautiful, witty, intelligent, and who knows the location of Pammel grocery); to Bernie my thanks for his unfailing good humor and my apologies for not believing his tale of being the illegitimate great grandson of Tsar Nicholas II. If you'd only mentioned the hemophilia I would never have asked you to hand me that razor blade. Wherever you are Bernie, I'm sorry (Bernard I, Tsar of all the Russias. It does have a ring to it.). And to Dean my admiration for proving there is life without chemistry.

To my father I extend my special thanks for always being ready to help. As he thumbs through this thesis I'm sure he will be overwhelmed with emotion as he realizes it cost him about $200 per page.

To my major professor, Ed Yeung, I offer my sincere appreciation for the encouragement, ideas, and insight provided during my graduate career, and for his personal composure when, with each succeeding quarterly report, he was reminded that more than just 1800 miles separate Ames and Berkeley.

Finally, to Ann and Noah, whose love and encouragement are an integral part of whatever success I may achieve, this thesis is dedicated.

APPENDIX A

In chapter one it was shown that the inverse Raman absorption coefficient was essentially constant over the interaction length when $P_s(0) >> P_L(0)$. Here we will examine the error incurred in assuming a constant absorption coefficient for purposes of data treatment when $P_s(0) \simeq P_L(0)$.

When $P_s(0) \simeq P_L(0)$ we must consider the absorption coefficient's dependence upon path length. Thus we may write:

$$\int_0^{\ell} g(z)dz = K \int_0^{\ell} P_s(z)dz \qquad \text{(A-1)}$$

where $K \equiv g(z)/P_s(z)$. In order to render the mathematics tractable, it will be assumed that we are in the regime where the exponentials in equations 2 and 17 can be replaced by the first two terms in their expansions (which is usually the case). Thus:

$$P_s(z) = P_s(0)\left\{1 + \int_0^z G(z')dz'\right\} \qquad \text{(A-2)}$$

Since $G(z')$ depends directly on $P_L(z')$, we may write:

$$G(z') = CP_L(0)\left\{1 - \int_0^{z'} g(z'')dz''\right\} \qquad \text{(A-3)}$$

where $C \equiv G(z')/P_L(z')$. To evaluate the above expression we assume that $g(z'')$ can satisfactorily be approximated by the mean absorption per unit path length, i.e.:

$$g(z'')\ell = \int_0^{\ell} g(z)dz \equiv \alpha \tag{A-4}$$

where α is obtained experimentally. Using the above two expressions, equation A-2 can readily be evaluated.

$$P_s(z) = P_s(0)\{1 + G(0)z - aG(0)z^2\} \tag{A-5}$$

where $a = \alpha/2\ell$. The first two terms in brackets represent, in the absence of any other effects, a constant linear gain. The term quadratic in z reflects the fact that the gain decreases as $P_L(z)$ attenuates. Substituting equation A-5 into A-1 and using equation 20 from chapter one we obtain:

$$\int_0^{\ell} g(z)dz = g(0)\ell\{1 + bg(0)\ell\} = \alpha \tag{A-6}$$

where:

$$b = (1/6)\{P_L(0)/P_s(0)\}(\sigma_s/\sigma_L)(3 - \alpha) \tag{A-7}$$

We note that when $P_s(0) >> P_L(0)$ the term in brackets in equation A-6 is essentially unity and the absorption coefficient can be considered constant in agreement with the discussion in chapter one. One will observe that b vanishes

when $\alpha = 3$. However, the assumptions underlying equation A-6 will breakdown long before α reaches a value of three and the above treatment will no longer be valid.

Evaluating equation A-6 for the specific case where $\alpha = 0{\cdot}10$ and $\{P_L(0)/P_s(0)\} \simeq (\sigma_s/\sigma_L) \simeq 1$, we calculate $\alpha \simeq 1{\cdot}05g(0)\ell$. If the Stokes power is measured after the sample cell, we will calculate $g(\ell)$ not $g(0)$. Assuming $\ell = 10$ cm, and using the fact $g(\ell)/g(0) = P_s(\ell)/P_s(0)$, equation A-5, along with equation 20, gives $g(\ell) \simeq 1{\cdot}1g(0)$. In summary the above example gives:

$$\int_0^{\ell} g(z)dz \simeq 1{\cdot}05g(0)\ell \simeq 0{\cdot}95g(\ell)\ell \qquad \text{(A-8)}$$

The relationships expressed in A-8 are a special case of the general relationship:

$$g(0)\ell \leq \int_0^{\ell} g(z)dz \leq g(\ell)\ell \qquad \text{(A-9)}$$

Expression A-8 indicates that, under the assumed conditions, an error of about 5% will be incurred by assuming a constant absorption coefficient. System characteristics (e.g., number density, Raman cross section) calculated assuming an absorption coefficient of $g(0)$ will be about 5% too high while those calculated

assuming an absorption coefficient of $g(\ell)$ will be about 5% too low.

APPENDIX B

In this section a brief derivation of the equation for the pressure change in a gas resulting from inverse Raman absorption will be presented. A similar equation has been used by West et al. (66).

In the regime where the p-V-T behavior of a gas can be satisfactorily represented by the ideal gas relationship we find that:

$$\Delta p = (\gamma - 1)U/V \qquad \text{(B-1)}$$

where γ is the heat capacity ratio (C_p/C_v) of the gas, V is the cell volume, and U is the thermal energy deposited in the gas (adiabatic conditions are assumed). If more than one gas is present, γ can be calculated using a partial pressure weighted average C_p and C_v.

For example, if we consider an ideal monatomic gas where $\gamma = 5/3$ and $U = \Delta E_T$, i.e., there are no internal degrees of freedom thus all of the thermal energy is channeled into translational energy E_T; we find using equation B-1:

$$\Delta p = 2\Delta E_T/3V \qquad \text{(B-2)}$$

a familiar result for ideal monatomic gases. For real molecular gases the $(\gamma - 1)$ term will correct for the

loss of energy to internal modes where it will not contribute to a pressure change.

To use equation B-1 it is necessary to determine U for inverse Raman absorption. The total energy, U_L, removed from the excitation beam as a result of inverse Raman absorption is:

$$U_L(J) = A\tau P_L(0)(1 - e^{-g\ell}) \qquad \text{(B-3)}$$

where $A(cm^2)$ is the cross sectional area of the interaction region, $\ell(cm)$ is the length of the interaction region, $\tau(sec)$ is the interaction time, $P_L(0)$ is expressed in $watts/cm^2$, and $g(cm^{-1})$ is given by equation 16. In the regime of low absorption equation B-3 can be approximated by:

$$U_L(J) = A\tau P_L(0)g\ell \qquad \text{(B-4)}$$

The energy which appears as thermal energy in the gas is not U_L, however, but rather the energy that results from the relaxation of the vibrational level populated by the inverse Raman process. Assuming all of the energy in the Raman excited vibrational level degrades to thermal energy we find:

$$U(J) = U_L(J)\Delta\sigma_R/\sigma_L \qquad \text{(B-5)}$$

where $\Delta\sigma_R(cm^{-1})$ is the Raman shift of the vibrational level and $\sigma_L(cm^{-1})$ is the energy of an excitation photon. Thus:

$$\Delta p(J/cm^3) = (\gamma - 1)A\tau P_L(0)g\ell\Delta\sigma_R/V\sigma_L$$
$$= K(\gamma - 1)A\tau\delta\ell P_L(0)\Delta\sigma_R N(d\sigma/d\Omega)/Vn_s^2\sigma_s^4\Delta\sigma \quad (B\text{-}6)$$

where $K = 5{\cdot}6 \times 10^{11}$. When a modulated cw source is used τ is the reciprocal of the modulation frequency.

Rigorously, equation B-6 is valid only for collimated beams of uniform irradiance in spatial coincidence at all points in the interaction region. The use of focused Gaussian beams with different waist diameters will lead to a mismatch in beam overlap which can be corrected for by performing radial and axial integration over the two beams in the interaction region. Unless the mismatch is severe, equation B-6 can be used to provide a good indication of the magnitude of the pressure change that can be expected.

For convenience, the following relationships are noted:

$$\Delta p(\mu bar) = \Delta p(J/cm^3) \times 10^7$$
$$\Delta p(Pa) = \Delta p(J/cm^3) \times 10^6$$
$$\Delta p(atm) = \Delta p(J/cm^3) \times 9{\cdot}87$$

APPENDIX C

In chapter three the detection of inverse Raman absorption using polarization rotation was discussed. In this section an equation will be obtained for the intensity of the field passing through the second polarizer. Only the case where both fields are linearly polarized will be considered.

Figure 12 shows the relationship between the two sets of coordinate axes used. The unit vectors $\hat{p}_1$ and $\hat{p}_2$ are parallel to the polarization directions of the fields passed by the first and second polarizers, respectively. These polarizers are crossed, i.e.:

$$\hat{p}_1 \cdot \hat{p}_2 = 0 \tag{C-1}$$

The electric vector of the excitation field in the sample, $\vec{E}_L$, (having passed through the first polarizer) is:

$$\vec{E}_L = E_L \hat{p}_1 \tag{C-2}$$

The electric vector of the Stokes field in the sample, $\vec{E}_s$, is:

$$\vec{E}_s = E_s \hat{s}_1 \tag{C-3}$$

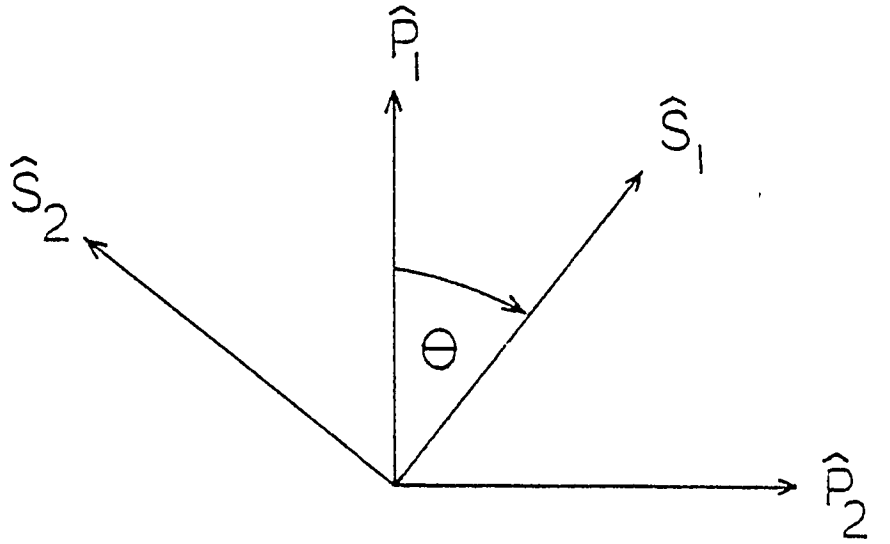
$\hat{p}_1$
$\hat{s}_1$
$\hat{s}_2$
θ
$\hat{p}_2$

where the frequency functionality of the fields has been suppressed. The intensity of a field will be given by:

$$I = \vec{E} \cdot \vec{E} \tag{C-4}$$

To treat the rotation, we reexpress $\vec{E}_L$ in the coordinate system of the Stokes field, i.e.:

$$\begin{aligned} \vec{E}_L &= E_L\{(\hat{p}_1 \cdot \hat{s}_1)\hat{s}_1 + (\hat{p}_1 \cdot \hat{s}_2)\hat{s}_2\} \\ &= E_L(1)\hat{s}_1 + E_L(2)\hat{s}_2 \end{aligned} \tag{C-5}$$

We thus consider the excitation field to be composed of two fields of identical frequency, propagation direction and phase, polarized orthogonally with intensities $\{E_L(1)\}^2$ and $\{E_L(2)\}^2$.

After passing through the sample each component field will be attenuated by the absorption induced by the Stokes field. Thus:

$$\begin{aligned} I_{L1}(\ell) &= I_{L1}(0) \exp\{-g_1\ell\} \\ I_{L2}(\ell) &= I_{L2}(0) \exp\{-g_2\ell\} \end{aligned} \tag{C-6}$$

where, using equation 31:

$$\begin{aligned} g_1 &= g/(1 + \rho) \\ g_2 &= g\rho/(1 + \rho) \end{aligned} \tag{C-7}$$

where g is given by equation 16 and ρ is the depolarization ratio of the Raman transition.

Using equations C-4, C-5, and C-6 one deduces that the electric vector of the excitation field after passing through the sample, $\vec{E}_L'$, can be written:

$$\vec{E}_L' = E_L\{e^{-\alpha}(\hat{p}_1 \cdot \hat{s}_1)\hat{s}_1 + e^{-\beta}(\hat{p}_1 \cdot \hat{s}_2)\hat{s}_2\} \quad \text{(C-8)}$$

where:

$$\alpha = g_1 \ell/2$$
$$\beta = g_2 \ell/2 \quad \text{(C-9)}$$

The intensity of the excitation field leaving the sample cell, $I_L(\ell)$, can be obtained from equation C-8.

$$I_L(\ell) = \vec{E}_L' \cdot \vec{E}_L' = I_L(0)\{e^{-2\alpha}\cos^2\Theta + e^{-2\beta}\sin^2\Theta\} \quad \text{(C-10)}$$

The intensity of the field passed by the second polarizer, I_L'', is readily given by:

$$I_L'' = (\vec{E}_L' \cdot \hat{p}_2)^2 = I_L(0)(e^{-\alpha} - e^{-\beta})^2\sin^2\Theta\cos^2\Theta \quad \text{(C-11)}$$

which for low absorption becomes:

$$I' \simeq I_L(0)(g\ell/4)^2\{(1 - \rho)/(1 + \rho)\}^2\sin^2 2\Theta \quad \text{(C-12)}$$

Application of simple differential calculus to equation C-11 shows that maximum sensitivity occurs when $\Theta = 45^\circ$.